
Article:
Asakura, T. and Williamson, M.P. orcid.org/0000-0001-5572-1903 (2023) A review on the structure of Bombyx mori silk fibroin fiber studied using solid-state NMR: an antipolar lamella with an 8-residue repeat. International Journal of Biological Macromolecules, 245. 125537. ISSN 0141-8130

https://doi.org/10.1016/j.ijbiomac.2023.125537

A review on the structure of *Bombyx mori* silk fibroin fiber studied using solid-state NMR: an antipolar lamella with an 8-residue repeat

Tetsuo Asakura[a] and Mike P. Williamson[b]

[a] Department of Biotechnology, Tokyo Univerrsity of Agriculture and Technology、2-24-16 Nakacho, Koganei Tokyo 184-8588, Japan;
E-mail: asakura@cc.tuat.ac.jp; Tel: +81-423-83-7733

[b] School of Biosciences, University of Sheffield, Firth Court,Western Bank, Sheffield S10 2TN, UK

Abstract:

Silk fibroin (SF) fiber from the silkworm *Bombyx mori* in the Silk II form has been used as an excellent textile fiber for over 5,000 years. Recently it has been developed for a range of biomedical appplications. Further expansion of these uses builds on the excellent mechanical strength of SF fiber, which derives from its structure. This relationship between strength and SF structure has been studied for over 50 years, but it is still not well understood. In this review, we report the use of solid-state NMR to study stable-isotope labeled SF fiber and stable-isotope labeled peptides including $(Ala\text{-}Gly)_{15}$ and $(Ala\text{-}Gly\text{-}Ser\text{-}Gly\text{-}Ala\text{-}Gly)_5$ as models of the crystalline fraction. We show that the crystalline fraction is a lamellar structure with a repetitive folding using β-turns every eighth amino acid, and that the sidechains adopt an antipolar arrangement rather than the more well-known polar structure described by Marsh, Corey and Pauling (that is, the Ala methyls in each layer point in opposite directions in alternate strands). The amino acids Ser, Tyr and Val are the next most common in *B. mori* SF after Gly and Ala, and occur in the crystalline and semi-crystalline regions, probably defining the edges of the crystalline region. Thus, we now have an understanding of the main features of Silk II but there is still a long way to go.

Keywords: *Bombyx mori* silk fibroin: Silk II structure: solid-state NMR: lamellar structure

1. Introduction

The silkworm *Bombyx mori* is a holometabolous insect: within about 50 days it goes through its complete life cycle consisting of four different metamorphosizing phases, namely egg or embryo, larva, pupa, and adult (moth).[1, 2] Of the life cycle, about half is the larval stage, which is the only stage at which the insects consume mulberry leaves. Although silk protein is produced throughout the larval state, except during molting, the largest amounts are synthesized in the fifth instar larval stage. This spinning stage is characterized by the extrusion of silk from spinnerets located in the head, and drawing of the fiber by a characteristic figure-eight head movement.

B. mori silk fibroin (SF) fiber possesses a combination of high tensile strength, large breaking strain and high toughness, which combine to make an outstanding material.[3-5] The fiber has been used to make high quality textiles for more than 5,000 years.[6] It has also long been used for surgical sutures in surgery. Recently, it has come to be recognized as an excellent biomaterial with a wide range of potential applications.[4,7-18] The relationship between strength and SF structure has been studied for over 50 years. As a result, great progress has been achieved. However, a clear understanding of this relationship is still lacking, because the SF structures proposed so far are not convincing. SF is a composite structure, consisting of alternating crystalline and amorphous domains. This means that X-ray diffraction analysis gives only limited structural information.[19-26] Other spectroscopic methods have also been applied to elucidate its structure,[6] but the most detailed structural information has been obtained by NMR, especially solid-state NMR.[27] SF in the solid state has been shown to adopt two quite different structures. Silk I is the structure of the SF stored in the middle silk glands and dried without any external forces, while Silk II is the structure of the crystalline part

of the fiber after spinning.[21] The main structured part of Silk I, Silk I*, is a repeated type II β-turn, which has been reviewed in detail in ref.28.

In this review, we describe our current understanding of the Silk II structure of SF fibers, mainly developed using various solid-state NMR techniques, and show that it adopts a lamellar structure (that is, the chain folds into a series of layers) with a repetitive folding made up from β-turns every eighth amino acid; and that the alanine sidechains are in an antipolar arrangement, meaning that within each layer, adjacent strands have sidechains pointing in opposite directions. Furthermore, we describe the structure of the Ser, Tyr and Val residues in SF in the Silk II form. It is important and timely to review in detail the lamellar structure, because a better understanding will guide developments in silk bio-materials, which are becoming very active recently.

2. The primary structure of *Bombyx mori* silk fibroin

SF consists of two polypeptides: a light chain (L) and a heavy chain (H) linked together via a single disulfide bond at the C-terminus of the H-chain, forming a H-L dimer. The H-L dimer also binds to glycoprotein P25 in a ratio of about 6 : 1.[29-31] The H-chain is the major protein component and accounts for approximately 92% of the molecular weight of SF. The amino acid composition of the H-chain (in mol %) is mainly Gly (46%), Ala (30%), Ser (12%), Tyr (5.3%) and Val (1.8%).[32] The primary structure has a repetitive core that is composed of alternating arrays of 12 repetitive and 11 amorphous domains, made up almost entirely from four motifs as shown in Figure 1(I).[32,33]

Figure 1

Motif (i) consists of a highly repetitive AGSGAG sequence and makes up a large

fraction of the crystalline domains in the SF fibers. The AGSGAG sequence is repeated multiple times, as shown in Figure 1(II). There are a total of 433 repeats, constituting a total of 2,598 amino acid residues, out of the total number of 5263 amino acid residues in the H-chain. Therefore, almost half of SF is made from AGSGAG sequences. Motif (ii) is a less repetitive sequence containing aromatic and/or hydrophobic residues, mainly Tyr and Val in sequences such as GAGAGY and/or GAGAGVGY, comprising the semi-crystalline regions. Motif (iii) is similar to motif (i) except for the presence of an additional GAAS motif, and motif (iv) forms the amorphous regions that separate the domains and contain negatively charged, polar, bulky hydrophobic, and/or aromatic residues, e.g., TGSSGFGPYVANGGYSGYEYAWSSESDFGT. The properties of SF are basically derived from the combination of these four motifs, and the still unsolved problem is how these sequence motifs translate into higher order structures.

3. Silk I and Silk II forms of *Bombyx mori* silk fibroin

Two crystalline forms, Silk I and Silk II, have been proposed as polymorphs of SF.[21] Silk I is the structure adopted by SF extracted from the middle silk glands in mild conditions and dried. It is not fibrous, because it has to be extruded from a liquid form, although it is clearly already well ordered. The main ordered conformation of Silk I (Silk I*), which is adopted by the regular repeat sequences such as motif (i), is a repeated type II β-turn (Figure 2). The structure was determined using a range of solid-state NMR techniques, with a combination of stable-isotope labeled SF and model

Figure 2

peptides, in particular $(AG)_{15}$, which is a good model for the typical sequence of the crystalline domain of SF.[34-48]

On spinning, silk fibroin forms a fiber comprised of crystalline units embedded in an amorphous matrix. It is presumably this composite structure that gives the fiber its outstanding mechanical properties. The crystalline units are composed of layers of antiparallel β-sheets, and are likely to be formed from Silk II nanocrystals (of a few nm in each direction) packed together into semi-crystalline arrays, with the regions between the nanocrystals being made largely from the semicrystalline sequences (motif (ii) from Figure 1).[27] It is possible to prepare a crystalline fraction (Cp) from SF fibers by chymotrypsin digestion of whole SF, which corresponds approximately with the nanocrystals.

A model of Silk II was first proposed by Marsh, Corey, and Pauling[19] using X-ray fiber diffraction (Figure 3(I)). Their model was an antiparallel (AP) β-sheet with the

Figure 3

sidechains in a polar arrangement. This means that one layer has all its alanine methyls facing down (the top layer with magenta methyls in Figure 3(I)); the next one has all methyls facing up (orange methyls in Figure 3(I)); and so on. The layers are thus grouped in pairs, with an Ala face and a Gly face (Figure 3(IIA)). However, subsequent studies using X-ray diffraction[20-23] showed a less regular structure than proposed by this model, although the antiparallel β-sheet structure was accepted and is still a textbook example of β-sheet structure. For example, Takahashi et al.[23] conducted a detailed study using better X-ray diffraction data based on 35 quantified intensities, and proposed an antipolar AP β-sheet structure as shown in Figure 3(IIB). An antipolar AP β-sheet has two identical faces, and the three-dimensional lattice is built up by stacking layers on top of another, although there are several possible translations that can achieve this. In order to fit the experimental data, the Takahashi model consisted of a random mixture of

two unspecified translations, occupying the crystal site with a ratio of 1:2. Their model is a better fit to the experimental data than the Marsh model, but requires unreasonable lengths for the intermolecular hydrogen bonds between the NH···OC groups of Ala and Gly. Therefore, the Tahahashi model is energetically unstable, and a more energetically favorable model was required. Solid-state NMR was able to provide such a model.

Figure 4 shows the ^{13}C cross-polarization/magic-angle spinning (CP/MAS) NMR spectrum of the Ala Cβ carbons of native [3-^{13}C] Ala-SF fibers.[49,50] The spectrum

Figure 4

shows three types of alanines within the crystalline region, which is inconsistent with the homogeneous structure suggested by Marsh et al. using X-ray diffraction data,[19] and more in agreement with X-ray diffraction studies reported previously by other groups.[20-23] The three alanine signals from the Cp fraction[51] were assigned as 18% distorted β-turns (**t**), plus two different signals from β-sheets: 25% β-sheets **A**, and 13% β-sheets **B**, with **t**:**A**:**B** in a ratio approximately 1:2:1. In contrast, the non-crystalline domain (44% of the total signal) consists of 22% each of distorted β-turn and distorted β-sheets.[50] The assignment of each peak was based on previously reported conformation-dependent ^{13}C NMR chemical shifts.[34-37,52-55]

The Cp fraction constitutes more than half of the total SF, and is made up largely from repeats of the sequence AGSGAG. Peptides made from repeats of this sequence were therefore used as models for the crystalline regions of Silk II. Expansions of the Ala Cβ peaks in the ^{13}C CP/MAS NMR spectra of $(AGSGAG)_n$ (n = 4, 5, and 8) and of the Cp fraction are shown in Figure 5, along with the spectra of the simpler sequence $(AG)_m$ (m = 12, 15, and 25).[56,57] The ratios of each are 23.3–24.0% for

Figure 5

peak **B** (21.8 ppm), 44.0–45.4% for peak **A** (19.5 ppm), and 30.9–32.7% for peak **t** (16.5 ppm). The fractions of **t, A**, and **B** are again roughly 1:2:1, and are almost the same for the $(AGSGAG)_n$ and Cp fractions. In addition, the relative intensities of **t, A**, and **B** are also the same in the expanded Ala Cβ peaks of $(AG)_m$ (m = 12, 15, and 25) as they are in $(AGSGAG)_n$ and Cp fractions. This indicates that all these molecules are expected to have a similar lamellar structure consisting of repeated smaller units.

4. Silk II has an antipolar antiparallel β-sheet structure

Before considering the lamellar structure model in detail, we will consider the antipolar/polar packing of the lamellar structure as shown in Figure 3(II).

In order to distinguish between these models, we obtained $^1H-^1H$ distance information from double-quantum magic angle spinning (DQMAS) ^1H NMR spectra. In these spectra, only $^1H-^1H$ distances within about 4 Å give rise to observable cross-peaks.[58,59] A set of nine $^1H-^1H$ correlation signals from the ^1H DQMAS NMR spectrum of $(AG)_{15}$ is marked in Figure 6(Ia).[60] These signals were compared to the

Figure 6

distances calculated from the polar Marsh and antipolar Takahashi models. Figure 6(II) shows that the Gly $H\alpha_2$ protons in adjacent β-strands are very close to one another (about 2 Å) in the polar Marsh model and therefore a diagonal peak for Gly $H\alpha_2$ should be detected. However, in the antipolar model this distance is more than 4 Å, and therefore no peak is expected. This feature is difficult to distinguish from Figure 6(Ia) because the Gly $H\alpha_2$ and Ala Hα peaks have overlapping chemical shifts. We therefore synthesized deuterium-labeled $([2\text{-d}]AG)_{15}$ and acquired another DQMAS ^1H NMR spectrum (Figure 6(Ib)). There is clearly no Gly $H\alpha_2$ peak on the diagonal, now that the

Ala Hα signal at around 5.0 ppm has been removed. This observation provides very strong evidence that the polar model cannot be correct.[60] Other experimental $^{1}H-^{1}H$ distance data were also only compatible with the antipolar model. For example, the observed cross-peak (v) is between Gly $H\alpha_2$ and Ala Hα which is longer than 4 Å in the polar model, but about 2.4 Å in the antipolar model. In addition, observed cross-peaks (viii) and (ix) are from Ala Hβ to Gly $H\alpha_1$ and Hα2 which are longer than 4 Å in the polar model, but about 2.3 and 2.6 Å , respectively, in the antipolar model.[60] Thus, the $^{1}H-^{1}H$ distance information obtained from DQMAS ^{1}H NMR clearly demonstrates that Silk II is antipolar, not polar.

5. Lamellar Structure of Silk II shown using $(Ala\text{-}Gly)_{15}$ as model peptides

To obtain further structural information, we synthesized all fifteen possible $(AG)_{15}$ peptides with ^{13}C labeling of a single alanine methyl, and observed the [3-^{13}C]Ala Cβ peaks shown in Figure 7(I). We deconvoluted the Ala $^{13}C\beta$ peaks to measure the

Figure 7

fractions of the three components **t**, **A** and **B**, which are shown in Figure 7(II).[56] The fractions at the Ala Cβ peak of the N-terminal Ala residue, Ala^1, were 6.6% **B**, 35.4% **A** and 58.0% **t**, respectively, indicating that the N-terminal Ala residue was mainly random coil, although significant amounts of β-sheet structure were still observed. The fraction of turn (**t**) decreased sharply for alanines at positions 3, 5 and 7, and then increased at positions 9 and 11. Beyond that, the fraction decreased slightly and then increased to a second maximum at position 19. It then decreased again up to position 25 and remained almost constant at positions 27 and 29. Thus, there are two maxima in the **t** population observed at positions 11 and 19.[61,62] The population of peak **A**, assigned

to AP β-sheet, tends to change inversely with the population of peak **t** and there are correspondingly two minima at positions 11 and 19. Contrary to the behavior of peak **A**, the population of peak **B** is fairly constant throughout, except for position 1. These data implied a possible lamellar structure with repetitive folding predominantly through turns at positions 11 and 19, i.e. every eighth amino acid. However, this cannot be the only structure present in the Cp fraction, because if the lamellar structure has turns only at positions 11 and 19, the fractions of the peaks **t** should be 100% at these positions, whereas they were actually 31% and 34%, respectively, for [3-^{13}C]Ala-$(AG)_{15}$ peptides.

The obvious alternative model, as shown in Figure 8(A), is an ensemble

Figure 8

of eight possible lamellar structures (I) to (VIII), with repetitive folding by β-turns every eighth amino acid at all possible positions.[56] This model contains three local structures for Ala: in the turn, and two β-sheet positions (one in the middle of a strand and one close to the turn at the end of the strand) in a ratio of 2:1, which we label **A** and **B** respectively because this matches the observed intensities of Ala methyls (Figure 7). We assumed an antipolar packing arrangement as discussed above. The positions of the turns differ among the lamellar structures (I) to (VIII) as indicated in Figure 8. For instance, the Ala^{11} residue (indicated by a circle in Figure 8(I) to (IV)) is in a **t** position in (I). However, it is **A** in (II) and (III), and **B** in (IV). The position of Ala^{11} in structures (V) to (VIII) is the same as in (I) to (IV), ie **t**, **A**, **A** and **B** respectively. The stabilities of the lamellar structures from (I) to (VIII) are probably different and thus, it is hard to predict the fraction of each structure. However, if these 8 lamellar structures are equally likely, the fractions of the structures (I) plus (V), which are the two structures with **t** peaks at positions 11 and 19, should be 25%. But the observed populations of **t** at these

positions were 31% and 34%, respectively. These values are slightly higher than 25%, implying that structures (I) and (V) have somewhat higher probabilities than the others. If we average only for the central parts of $(AG)_{15}$, that is, positions 9 to 23, we calculate the percentages of the averaged fractions as 24.9 : 49.5 : 25.6 for **t** : **A** : **B**, respectively, which is very close to the observed 1 : 2 :1 distribution. Thus, we proposed a lamellar structure for the crystalline domain of SF fiber as shown in Figure 8(Bb). This has three types of Ala: two β-sheet positions **B** and **A**, and one β-turn **t**, with abundancies in the ratio 1 : 2 : 1. These peaks correspond to three Ala Cβ carbons with different spatial arrangements. In the extended part of the lamellar structure, two Ala Cβ carbons with the same arrangement are assigned to **A**, while the other one with a different arrangement is assigned to **B**. Thus, the NMR data are all consistent with an antipolar lamellar structure with repetitive folding through β-turns every eighth amino acid. It is worth noting that the observed ratios are only consistent with an 8-residue repeat, that has one turn, two central and one end β-sheet alanine in each strand.

We checked the lamellar structure using two other kinds of solid-state NMR experiments: ^{13}C spin diffusion NMR observation under off magic angle spinning [37,44,49,62-77] and rotational echo double resonance (REDOR).[37,39,44,76-80] Expansions of the carbonyl regions from the ^{13}C spin diffusion NMR spectra of (a) $(AG)_6A[1\text{-}^{13}C]G^{14}[1\text{-}^{13}C]A^{15}G(AG)_7$ and (b) $(AG)_8A[1\text{-}^{13}C]G^{18}[1\text{-}13C]A^{19}G(AG)_5$ observed under slow MAS condition are shown in Figure 9 together with the corresponding simulated

Figure 9

spectra, (c) and (d), and the calculated spectrum of (e) AP β-sheet (calculated using ϕ and φ = -150° and 150° respectively).[62] Comparing (a) and (b) with the spectrum (e),

which is the spectrum expected for a 100% AP β-sheet structure, it is immediately clear that the non-diagonal components in (a) and (b) are more enhanced, suggesting the presence of additional structures to the AP β-sheet structure in the peptide. In addition, spectrum (b) has a higher population of nondiagonal components than spectrum (a). We already know from Figure 7(II) that the population of distorted β-turn at A^{15} is 23%, but that of A^{19} is 34%. Therefore the increased nondiagonal component in spectrum (b) compared with that of the same peptide labeled at Ala^{15} in spectrum (a) is consistent with the proposed increased fraction of the distorted β-turn component.

REDOR experiments further confirmed this conclusion. REDOR measures the distance between two labeled nuclei very accurately. Experiments carried out on peptides doubly labeled with [^{13}C] and [^{15}N] at different locations are very useful for studying peptide and protein structures containing turns, because the measured atomic distance between C and N nuclei is shorter if these nuclei are in a turn.[37,62,81-83] Table 1 compares the observed interatomic distances between the labeling sites determined

Table 1

from REDOR plots, with the predicted averaged interatomic distances calculated from the percentage composition of β-turn and β-sheet at that location as determined by deconvolution of the Ala Cβ CP/MAS spectra (Figure 7(II)). If $(AG)_{15}$ adopts a pure β-sheet structure, all the interatomic observed distances should be longer than the distances determined by REDOR by 0.2-0.3 Å for the peptides D1-D4, and 0.8 Å for D5. However, by including the measured fraction of β-turn structure, the predicted distances become in much better agreement with the observed distances. Thus, the results from REDOR are in good agreement with those from the Ala Cβ CP/MAS NMR

spectra, providing strong supporting evidence for the existence of a combination of β-turn and β-sheet secondary structure at Ala^{15} in $(AG)_{15}$.

The REDOR experiment can also be used to obtain information about the intermolecular arrangement.[56] $[^{15}N]Ala^{1}G(AG)_{13}A[1\text{-}^{13}C]Gly^{30}$ was synthesized; this labeling pattern (with the labels at the extreme ends of the peptide) was chosen because the ^{15}N and ^{13}C sites are too far apart to produce an intramolecular REDOR effect, so any REDOR effect observed must necessarily arise from the intermolecular arrangement of the $(AG)_{15}$ lamellar structures. The optimal fitted distance from the REDOR measurements was 4.4 Å, which is a short enough atomic distance to derive from head-to-tail ordering of two lamellar molecules. That is, the N-terminal NH_3^+ group of $[^{15}N]Ala^{1}$ in the lamellar molecule forms an intermolecular hydrogen bond with the C-terminal CO_2^- group of $[1\text{-}^{13}C]Gly^{30}$ of another lamellar molecule through head-to-tail ionic bonding.

The model proposed here is not the only lamellar structure possible. Tirrell's group have reported the use of genetic engineering to produce artificial proteins that adopt predictable, chain-folded AP β-sheet structures in the solid state.[84-86] The chain-folded lamellar architecture is a kinetic trap in the crystallization of all linear polymers sufficiently flexible to form hairpin-like folds, and it is well established that hairpin turns in β-strands can form with either one or two amide groups in the turn, which are known as γ and β-turns respectively.[87] Panitch et al.[88] produced $(AG)_{64}$ peptides from recombinant *Escherichia coli* using genetic engineering and recrystallized them from dichloroacetic acid solutions as chain-folded lamellae with a lamellar stack periodicity of 32 Å. The structure consists of polar AP β-sheets folding by means of γ-turns. The

sheets stack in pairs with Ala faces together and Gly faces together, with a stacking periodicity about 3% greater than that reported previously by Fraser et al.[89,90] where chain folding was not evident. To obtain good agreement between the calculated and observed X-ray structure factors, successive sheets must shear randomly by ± ***a***/4 and ± ***c***/2 in the ***ac*** plane. The final structure is shown in Figure 10 [88,91] which has similarities

Figure 10

to our proposed lamellar structure. However, there are significant differences between the two lamellar models: Their model has polar stacking and γ-turns, whereas ours has antipolar stacking and β-turns. As mentioned above, our proposed lamellar model was based on $^{1}H-^{1}H$ distance information from the observed DQMAS ^{1}H NMR spectra, and the polar stacking model cannot explain the observed distance data. A further argument in favor of our model is that a β-turn has two residues in the turn and naturally produces an antipolar structure (Figure 8), whereas a γ-turn has one residue in the turn and naturally produces a polar structure. The structure of the turn and the polar/antipolar character are thus tightly linked. Finally, we have shown that Silk I consists of repeated β-turns (Figure 2). It seems more natural for the refolding of Silk I to Silk II (which takes place in the spinneret arising from shear stress, dehydration and a reduction in pH) to retain the β-turns rather than change completely to γ-turns. We therefore conclude that our model is the most consistent with the available experimental data.

6. Serine in the (Ala-Gly-Ser-Gly-Ala-Gly) repeats does not alter the structure

So far, we have considered only the Gly and Ala residues in SF. We showed above that the most common motif in SF is the sequence AGSGAG. We therefore discuss here solid-state NMR experiments on $(AGSGAG)_5$ peptides, which should be a better mimic

of the Cp fraction of SF fiber than $(AG)_{15}$. We used a similar strategy to that described above: $(AGSGAG)_5$ peptides were synthesized with all ten possible [3-^{13}C]Ala labels, and the ^{13}C CP/MAS NMR spectra were deconvoluted to give the populations of each component.[57] Figure 11(I) shows the results, while Figure 11(II) shows the resulting

Figure 11

populations. The results are similar to those shown in Figure 7: the fractions of peaks **A** and **B** corresponding to AP β-sheet changed inversely with the fraction of peak **t**. The minima at positions 11 and 19 indicate that these regions formed turns. The decrease in peak **t** at positions 5 to 7, and 23 to 25, and the concomitant increase in peak **A**, suggests that these regions form AP β-sheet rather than distorted β-turn. This pattern indicates a lamellar structure of $(AGSGAG)_5$ with a repetitive folding predominantly through turns at positions 11 and 19, i.e. every eighth amino acid. Thus, the lamellar structure of $(AGSGAG)_5$ is similar to that of $(AG)_n$, and it is likely to be an excellent model for the Cp fraction. The replacement of Ala by Ser has a rather small overall effect on the structure of the chain.

Based on these observations, and the 1:2:1 ratio for the **t**:**A**:**B** Ala Cβ peaks, a model of the lamellar structure of $(AGSGAG)_5$ was proposed, as shown in Figure 12. We

Figure 12

also compared the plots for $(AG)_{15}$ and $(AGSGAG)_5$, and observed that the populations of the distorted β-turn and/or random coil component were higher in $(AGSGAG)_5$ than they are in $(AG)_{15}$, except for the two Ala residues at the N-terminal end. This suggests that the presence of repeated Ser residues in the peptide chain may result in some disturbance to the lamellar structure. In support of this hypothesis, we cited the data from Fraser et al.[89,90] who reported that the unit cell dimensions of $(AG)_n$ and

$(AGAGSG)_m$ were different in the ***c***-axis, which is in the direction perpendicular to the plane of the sheet. They showed that the side chains of Ser residues in $(AGSGAG)_5$ stick out perpendicularly to the plane of the β-sheet, producing a larger ***c***-spacing beween lamellae compared to $(AG)_{15}$. This larger separation allowed looser, less regularly located turns in the lamellar structure. We will examine the local structure and dynamics of Ser residue in $(AGSGAG)_5$ in the Silk II form in detail in the next section.

Finally, the angle of the Cα-H_2 bonds of Gly and the Cα-CβH_3 bond of Ala relative to the fiber axis was determined using [2,2-$^2H_2$]Gly- or [3,3,3-$^2H_3$]Ala-SF fiber samples studied by ^{2}H solid-state NMR.[92,93.] Uniaxially aligned block samples were prepared from [2,2-$^2H_2$]Gly- or [3,3,3-$^2H_3$]Ala-SF fibers, and ^{2}H solid-state NMR spectra were recorded as a function of the tilt angle α between the fiber axis and external magnetic field. A tilt series of these spectra is shown in Figure 13(I), and compared to line-shape simulations. The agreement

Figure 13

between the experimental and simulated spectra is good when the angle between the α-$^2H_2$ bond of Gly and the fiber axis was fixed at 90°, indicating that the direction of the Cα-$^2H_2$ bond of Gly residue is perpendicular to the fiber axis as shown in Figure 13(I). Similarly, the direction of the Cα-Cβ$^2H_3$ bond of Ala residue is also perpendicular to the fiber axis (Figure 13(II)). This result further confirms the general correctess of our model.

7. Local structure and dynamics of Ser in the Silk II crystalline region

In previous sections, we have discussed in some detail the three signals seen for Ala

Cβ in the crystalline fraction Cp, which we assigned to a distorted β-turn **t** and two β-sheet signals **A** and **B**. Ser Cα and Cβ peaks are also split into multiple components. In order to assign them, we used two-dimensional ^{13}C-^{13}C dipolar assisted rotational resonance (2D ^{13}C-^{13}C DARR) experiments.[94-102] 2D DARR cross peaks indicate short- and long-range through-space dipolar contacts between ^{13}C spins, such that a short mixing time shows short distances, and a longer mixing time shows longer distances. Figure 14(I) shows a 2D ^{13}C-^{13}C DARR spectrum of the [U-^{13}C] Cp fraction observed

Figure 14

at a short mixing time of 10 ms.[103] The cross peaks between Ser Cα and Ser Cβ can only be intra-residue with such a short mixing time. Four such cross peaks are clearly observed: hereafter we abbreviate them by their chemical shifts as (i) (Cα 55.6, Cβ 66.8), (ii) (Cα 54.9, Cβ 64.2), (iii) (Cα 54.0, Cβ 63.5) and (iv) (Cα 56.0, Cβ 61.4). Three of these peaks have Cβ chemical shifts larger than that of the typical AP β-sheet chemical shift of 62.8 ppm.[104] The larger chemical shift is attributed to an inter-sheet packing effect, probably similar to the effect that produces separate **A** and **B** shifts for Ala Cβ. In contrast, the cross peak (iv) (Cα 56.0, Cβ 61.4) is attributable to random coil because both chemical shifts are in agreement with the ^{13}C solution NMR chemical shifts of Ser Cβ in proteins with random coil conformation in aqueous solution.[105] Figure 14(II) shows the correlations between Ala Cβ and Ser in the DARR spectrum with a long mixing time of 400 ms.[103] The peaks of Ser Cα at 54.9 and 54.0 ppm correlate with the peaks of Ala Cβ at 19.6 (**A**) and 21.7 (**B**) ppm, respectively. Moreover, the Ser peak of Cβ at 64.2 ppm has a strong cross peak with the peak of Ala Cβ **A**, while the peaks of Ser Cβ **B** are too weak to interpret. These observations

allowed us to assign the four sets of Sα and Sβ peaks of the Cp fraction, and to determine their fractions by deconvolution of the Cβ peak as (i) 10% distorted β-sheet **A**, (ii) 37% β-sheet **A**, (iii) 12% β-sheet **B** and (iv) 41% random coil.

Next, we studied the dynamics of Ser residues and the formation of interchain hydrogen bonds through the Ser OH side chain. Figure 15(I) shows a measurement of

Figure 15

the ^{13}C spin lattice relaxation time (T_1^C) of the four components (66.8 ppm, 64.2 ppm, 63.5 ppm and 61.4 ppm) of the Ser^{15} Cβ peak of [3-^{13}C]Ser^{15}-$(AGSGAG)_5$, which can be used to analyze their mobility.[106] The log plots of peak intensity versus delay time (Figure 15(I)) show that three of the four peaks have multiple T_1^C components. For each of these, we fitted the plots to two exponential decays, and obtained the ratio and T_1^C values of the shorter and longer relaxation time components ($T_1^C{}_{short}$ and $T_1^C{}_{long}$).[83, 92, 107, 108] Table 2 and Figure 15(II) summarize the results. From previous measurements of

Table 2

T_1^C carried out different temperatures, it is known that the Ser Cβ peaks have a mobility in the strong collision limit, which means that the components with the longer T_1^C values indicate a lower molecular mobility.[83] Only the peak at 63.5 ppm (assigned as **B**; Figure 14(II)) was found to be a single component, with the longest T_1^C value among the Ser Cβ peaks (Table 2 and Figure 15(II)), which means that this peak has a rigid conformation, likely to arise from strong hydrogen bonds involving the Ser side chain OH. On the other hand, in the main β-sheet peak at 64.2 ppm, the longer T_1^C component was minor and the relaxation value was the shortest (Table 2 and Figure 15(II)). This peak has been assigned as a β-sheet **A** peak on the basis of its strong correlation with

Ala Cβ **A** (Figure 14(II)). These results suggest that Ser residues close to **A** (ie, in the center of the lamellar β-strand) are relatively stable but do not form stable hydrogen bonds with other chains. Interestingly, the random coil peak showed more percentage of the longer T_1^C component. This shows that in the random coil structure, the percentage of hydrogen-bonding conformation is larger than that for **A**. It is worth noting that in a liquid NMR spectrum, random coil structure usually implies an isotropically mobile component, whereas in solid-state NMR spectra of materials with high hydrogen-bonding networks, random coil structure does not always mean a mobile component.

Ser occurs every sixth residue in the crystalline region, but the lamellar structure folds every eighth residue, implying that Ser is distributed regularly throughout the crystalline region. 68% of the Ser in silk fibroin is in $(AGSGAG)_n$ repeats, highlighting their importance to the crystalline structure. In the center of the lamellar strand (residues **A**), Ser is not rigid and Ala methyls are relatively mobile. However, at the edges of the strands (residues **B**), Ser is more hydrogen bonded, and Ala methyl groups have more restricted motion.[57] We infer that a major function of the Ser is to hold the edges of the nanocrystals together, forming hydrogen bonds between one lamellar layer and the next. They may also link together neighboring nanocrystals, as implied by the high degree of hydrogen bonding in the non-crystalline signals.

8. The structure of Tyr and Val residues in the semi-crystalline region of Silk II

Tyr and Val residues are the 4th and 5th most common amino acids of SF. The fraction of Tyr is 5.2% and that of Val is 1.8% in the H chain. Zhou et al.[32,33] showed that in addition to the repeating sequence of GAGAGS (Motif (i)), the primary sequence of SF also contains Motif (ii). Motif (ii) is a less repetitive sequence containing aromatic

and/or hydrophobic residues such as GAGAGY and/or GAGAGVGY, comprising the semicrystalline regions. Thus, it is interesting to study the structures of these residues in SF fiber. Figure 16(I) shows ^{15}N NMR solution spectra (80-110 ppm) of selectively

Figure 16

^{15}N-labeled SF samples: (a) [^{15}N]Val-SF, (b)[^{15}N]Tyr-SF, and (c) [^{15}N]Ser-SF. For comparison, the ^{15}N NMR spectrum of non-labeled SF sample is also shown (d).[109] These ^{15}N labeled SF samples were prepared by culturing *B. mori* posterior silk glands from 4-day-old, fifth instar larvae using a rotation culture procedure with modified Grace's insect medium, containing the relevant ^{15}N-labeled amino acids, while oxygenating the medium.[110] Sufficient labeled samples were obtained for [^{15}N]Tyr- and [^{15}N]Ser-SF. Although relatively low enrichment of [^{15}N]Val-SF sample was produced due to the low proportion of Val residues in SF, the [^{15}N]Val peak is still enriched enough to be useful. Therefore, all these selectively labeled samples can be used for ^{15}N solid-state NMR analysis. To gain insight into the structural organization of the SF molecules, we investigated the ^{15}N solid-state NMR spectra of [^{15}N]Tyr-, [^{15}N]Val-, and [^{15}N]Ser-SF fibers in the Silk II form. Oriented samples were obtained as blocks, which were placed with the fiber axis either parallel or perpendicular to the magnetic field as shown in Figure 16(II).[111] All of the experimental spectra were found to contain a contribution of approximately 30% of a non-oriented powder pattern which was subtracted from the observed spectra. The resulting spectral patterns in Figure 16(II) show significant differences between the parallel and perpendicular alignments, indicating that the Tyr and Val sites are well-aligned within the macroscopic fiber. Since the spectral patterns are very similar to those of [^{15}N]Gly- and [^{15}N]Ala-labeled SF samples reported previously,[111] we conclude that Tyr and Val residues in motif (ii)

form AP β-sheet structure within the semicrystalline domain, similar to the Ser residues in the crystalline domain of motif (i).

In order to expand on this observation, we obtained the ^{13}C CP/MAS NMR spectra of (A) [3-^{13}C]Tyr- and [3-^{13}C]Ser-SF before spinning, (B) non-labeled SF before spinning and (C) [3-^{13}C]Tyr- and [3-^{13}C]Ser-SF fiber after spinning as shown in Figure 17(I).[112]

Figure 17

The Tyr Cβ peak is difficult to analyze, because of overlap with the natural abundance Gly Cα peak. Therefore, the fractions of the different conformations of Tyr residues were determined by simulation of the difference spectra by subtracting the non-labeled spectrum from the ^{13}C-labeled spectrum. The populations of Tyr were measured after peak deconvolution as 92% random coil and 8% β–sheet for the sample before spinning, and 44% random coil and 56% β-sheet after spinning. Thus, more than half of the Tyr adopt β-sheet structure. Figure 17(II) shows the Val $^{13}C\alpha$ peak obtained by subtracting non-labeled SF fiber from [2-^{13}C]Val-SF fiber. The ^{13}C chemical shift of Val $^{13}C\alpha$ peak in Figure 17(II) was about 57.5 ppm, indicating that the conformation is also predominantly β-sheet structure.[109]

As shown in Figure 4, the fraction of non-crystalline domain in SF is 44%. It consists of 22% each of distorted β-turn and distorted β-sheets. We synthesized the main sequences in Motif (ii), i.e., $(AGYGAG)_5$,[113] $(AGAGYGAGAG)_3$[113] and $(AG)_3YG(AG)_2VGYG(AG)_3YG(AG)_3$.[50] Then, we observed the ^{13}C CP/MAS NMR spectra of these sequences. Figure 17(III) shows expanded Ala Cβ peaks of the ^{13}C CP/MAS NMR spectra of (A) $(AGYGAG)_5$, (B) $(AGAGYGAGAG)_3$ and (C)

$(AG)_3YG(AG)_2VGYG(AG)_3YG(AG)_3$. These spectral patterns reproduce that of the non-crystalline domain obtained from the difference spectrum of Figure 17(III). Specifically, the fraction is 22% of both distorted β-turn and distorted β-sheets. Thus, the fraction agrees with the fraction of Tyr residues in the SF fiber mentioned above. This result is unexpected because more than half of Motif (ii) forms a β-sheet structure in the SF fiber.

In summary, based on these results we propose that much of the backbone of the Tyr and Val residues (which occur in the semicrystalline region) has regular antiparallel β-sheet structure, but that the sidechains are less ordered than in the crystalline region. In Silk I, the Tyr act as 180° chain reversal points, and we speculate that they maintain this function in Silk II: in other words, that the Tyr are located at the edges of crystalline or semicrystalline regions, at 180° chain reversals. Tyr rings cannot be accommodated within the lamellar structure, but are functionally important.

9. Conclusions and Future Aspects

In this review, we proposed a chain-folded lamellar structure for *Bombyx mori* silk fibroin (SF) fiber based on solid-state NMR analysis of model peptides. We showed that the crystalline domain of SF consists of β-turns every eighth amino acid and that the chains adopt an antipolar arrangement. These proposals are based on multiple sets of experimental evidence, which provide unambiguous support and enable the community to move on to more detailed structural studies. We also studied the conformations of Ser in the crystalline domain, and Tyr and Val residues in the semicrystalline domain. However, many limitations remain, including a lack of direct evidence for the chain-folding mechanism from repeated type II β-turn structure in Silk I before spinning to a

lamellar structure in Silk II as reported here, as well as the influence of a range of environmental factors on the fiber structure, such as tensile and shear stress in the spinneret including in the silk press region of silkworm, loss of water molecules, the presence of silk sericin and metal ions, and liquid-liquid phase separation as evidenced by the formation of micron-scale liquid droplets. A greater understanding of these factors is needed before we can hope to produce suitably strong fibers synthetically. Therefore, we suggest further research is needed to address these issues and to explore the potential applications of SF fiber in various fields.

Funding: This research was funded by a JSPS KAKENHI, Grant-in-Aid for Scientific Research (C), Grant Number JP19K05609.

Institutional Review Board Statement: Not applicable.

Informed Consent Statement: Not applicable.

Conflicts of Interest: There is no conflict of interest associated with the authors of this paper.

References

1.Y Tazima (Ed.) The silkworm, Kodansha Scientific Books, Tokyo, 1978.

2. T Asakura, DL Kaplan, Ed. CJ Arutzen, Silk production and processing. Encyclopedia of Agricultural Science, Academic Press, London 1994, 4, pp.1-11.

3. Z Shao, F Vollrath, Surprising strength of silkworm silk. Nature 2002, 418, 741.

4. C Vepari, DL Kaplan, Silk as a Biomaterial. Prog. Polym. Sci. 2007, 32, 991-1007.

5. L-D Koh, Y Cheng, C-P Teng, Y-W Khin, X-J Loh, S-Y Tee, M Low, E Ye, H-D Yu,Y-W Zhang, M-Y Han, Structures, Mechanical Properties and Applications of Silk Fibroin Materials. Prog. Polym. Sci. 2015, 46, 86-110.

6. M Schoeser, The Science of Silk, Yale University press, 2007, pp.232-241.

7. Y Wang, HJ Kim, G Vunjak-Novakovic, DL Kaplan, Stem cell-based tissue engineering with silk biomaterials. Biomaterials 2006, 27, 6064-6082.

8. Q Zhang, S Yan, M Li, Silk fibroin based porous materials. Materials 2009, 2, 2276-2295.

9. E. Wenk, HP Merkle, L Meinel, Silk fibroin as a vehicle for drug delivery applications. J. Controlled Release 2011, 50, 128-141.

10. N Kasoju, U Bora, Silk fibroin in tissue engineering. Adv. Healthc. Mater. 2012, 1, 393-412.

11. H Tao, DL Kaplan, FG Omenetto, Silk materials – a road to sustainable high technology. Adv. Mater. 2012, 24, 2824-2837.

12. B Kundu, R Rajkhowa, SC Kundu, X Wang, Silk fibroin biomaterialsfor tissue regenerations. Adv. Drug. Deliv. Rev. 2013, 65, 457-470.

13. B Kundu, NE Kurland, S Bano, C Patra, FB Engel,VK Yadavalli, SC Kundu, Silk proteins for biomedical applications: bioengineering perspectives, Prog. Polym. Sci.

2014, 39, 251-267.

14. T Asakura, T Miller, Biotechnology of Silk; T Asakura, T Miller, Eds.; Biologically-Inspired Systems; Springer Netherlands: Dordrecht, 2014; Vol. 5.

15. AE Thurber, FG Omenetto, DL Kaplan, *In vivo* bioresponses to silk proteins, Biomaterials 2015, 71, 145-157.

16. RFP Pereira, MM Silva, V de Zea Bermudez, *Bombyx Mori* Silk Fibers: An Outstanding Family of Materials. Macromol. Mater. Eng. 2015, 300, 1171-1198.

17. C Holland, K Numata, J Rnjak-Kovacina, FP Seib, The biomedical use of silk: past, present, future, Adv. Healthc. Mater. 2018, 1800465.

18. AB Tamara, ET DeSimone, TR Scheibel, Biomedical applications of recombinant silk-based materials, Adv. Mater. 2018, 30, 1704636.

19. RE Marsh, RB Corey, L Pauling, An Investigation of the Structure of Silk Fibroin. Biochim. Biophys. Acta 1955, 16, 1-34.

20. B Fraser, TP MacRae, Conformations of Fibrous Proteins and Related Synthetic Polypeptides; Academic Press: New York, 1973.

21. B Lotz, F Colonna Cesari, The Chemical Structure and the Crystalline Structures of *Bombyx Mori* Silk Fibroin. Biochimie 1979, 61, 205-214.

22. SA Fossey, G Némethy, KD Gibson, HA Scheraga, Conformational Energy Studies of β-Sheets of Model Silk Fibroin Peptides. I. Sheets of Poly(Ala-Gly) Chains. Biopolymers 1991, 31,1529−1541.

23. Y Takahashi, M Gehoh, K Yuzuriha, Structure Refinement and Diffuse Streak Scattering of Silk (*Bombyx Mori*). Int. J. Biol. Macromol. 1999, 24, 127-138.

24. PE Bourne, H Weissig, editors. Structural bioinformatics. 1st ed.Chichester: John Wiley & Sons Inc.; 2003. p. 649.

25. RH Garrett, CM Grisham, Biochemistry. 3rd ed. Belmont: BrooksCole; 2007. p. 1086.

26. SL Chang, X-ray multiple-wave diffraction: theory and application.Berlin: Springer Series; 2010. p. 143-222

27. T Asakura, K Okushita, MP Williamson, Analysis of the Structure of *Bombyx Mori* Silk Fibroin by NMR. Macromolecules 2015, 48, 2345-2357.

28. T Asakura, Structure of Silk I (*Bombyx Mori* Silk Fibroin before Spinning) -Type II β-Turn, Not α-Helix. Molecules 2021, 26, 3706.

29. K Yamaguchi, Y Kikuchi, T Takagi, A Kikuchi, F Oyama, K Shimura, S Mizuno, Primary structure of the silk fibroin light chain determined by cDNA sequencing and peptide analysis. J. Mol. Biol. 1989, 210, 127-139.

30. K Tanaka, N Kajiyama, K Ishikura, S Waga, A Kikuchi, K Ohtomo, T Takagi, S Mizuno, Determination of the Site of Disulfide Linkage between Heavy and Light Chains of Silk Fibroin Produced by *Bombyx Mori*. Biochim. Biophys. Acta, Protein Struct. Mol. Enzymol. 1999, 1432, 92-103.

31. S Inoue, K Tanaka, F Arisaka, S Kimura, K Ohtomo, S Mizuno, Silk fibroin of *Bombyx mori* is secreted, assembling a high molecular mass elementary unit consisting of H-chain, L-chain, and P25, with a 6:6:1 molar ratio. J. Biol. Chem. 2000, 275, 40517-40528.

32. C-Z Zhou, F Confalonieri, N Medina, Y Zivanovic, C Esnault, T Yang, M Jacquet, J Janin, M Duguet, R Perasso, Z-G Li, Fine organization of *Bombyx mori* fibroin heavy chain gene. Nucleic Acids Res. 2000, 28, 2413-2419.

33. C-Z Zhou, F Confalonieri, M Jacquet, R Perasso, Z-G Li, J Janin, Silk Fibroin: Structural Implications of a Remarkable Amino Acid Sequence. Proteins 2001, 44, 119-122.

34. H Saitô, R Tabeta, T Asakura, Y Iwanaga, A Shoji, T Ozaki, I Ando, High-Resolution ^{13}C NMR Study of Silk Fibroin in the Solid State by the Cross-Polarization-

Magic Angle Spinning Method. Conformational Characterization of Silk I and Silk II Type Forms of *Bombyx Mori* Fibroin by the Conformation-Dependent ^{13}C Chemical Shifts. Macromolecules 1984. 17, 1405-1412.

35. T Asakura, A Kuzuhara, R Tabeta, H Saito, Conformational Characterization of *Bombyx Mori* Silk Fibroin in the Solid State by High-Frequency ^{13}C Cross Polarization-Magic Angle Spinning NMR, X-Ray Diffraction, and Infrared Spectroscopy. Macromolecules 1985, 18, 1841-1845.

36. T Asakura, M Demura, T Date, N Miyashita, K Ogawa, MP Williamson, NMR Study of Silk I Structure of *Bombyx Mori* Silk Fibroin with ^{15}N- and ^{13}C-NMR Chemical Shift Contour Plots. Biopolymers 1997, 41, 193-203.

37. T Asakura, J Ashida, T Yamane, T Kameda, Y Nakazawa, K Ohgo, K Komatsu, A Repeated β-Turn Structure in Poly(Ala-Gly) as a Model for Silk I of *Bombyx Mori* Silk Fibroin Studied with Two- Dimensional Spin-Diffusion NMR under off Magic Angle Spinning and Rotational Echo Double Resonance. J. Mol. Biol. 2001, 306, 291-305.

38. T Asakura, T Yamane, Y Nakazawa, T Kameda, K Ando, Structure of *Bombyx Mori* Silk Fibroin before Spinning in Solid State Studied with Wide Angle X-Ray Scattering and ^{13}C Cross-Polarization/magic Angle Spinning NMR. Biopolymers 2001, 58, 521-525.

39. T Gullion, R Kishore, T Asakura, Determining Dihedral Angles and Local Structure in Silk Peptide by ^{13}C ^{2}H REDOR. J. Am. Chem. Soc**.** 2003, 125, 7510-7511.

40. T Yamane, K Umemura, T Asakura, The Structural Characteristics of *Bombyx Mori* Silk Fibroin before Spinning as Studied with Molecular Dynamics Simulation. Macromolecules 2002, 35, 8831-8838.

41. P Monti, P Taddei, G Freddi, K Ohgo, T Asakura, Vibrational ^{13}C-Cross-Polarization/magic Angle Spinning NMR Spectroscopic and Thermal Characterization of Poly(alanine-glycine) as Model for Silk I *Bombyx Mori* Fibroin. Biopolymers 2003, 72, 329-338.

42. T Yamane, K Umemura, Y Nakazawa, T Asakura, Molecular Dynamics Simulation

of Conformational Change of poly(Ala-Gly) from Silk I to Silk II in Relation to Fiber Formation Mechanism of *Bombyx Mori* Silk Fibroin. Macromolecules 2003, 36, 6766-6772.

43. P Taddei, T Asakura, J Yao, P Monti, Raman Study of Poly(alanine-glycine)-Based Peptides Containing Tyrosine, Valine, and Serine as Model for the Semicrystalline Domains of *Bombyx Mori* Silk Fibroin. Biopolymers 2004, 75, 314-324.

44. T Asakura, K Ohgo, K Komatsu, M Kanenari, K Okuyama, Refinement of Repeated β-Turn Structure for Silk I Conformation of *Bombyx Mori* Silk Fibroin Using ^{13}C Solid-State NMR and X-Ray Diffraction Methods. Macromolecules 2005, 38, 7397-7403.

45. T Asakura, K Ohgo, T Ishida, P Taddei, P Monti, R Kishore, Possible Implications of Serine and Tyrosine Residues and Intermolecular Interactions on the Appearance of Silk I Structure of *Bombyx Mori* Silk Fibroin-Derived Synthetic Peptides: High-Resolution ^{13}C Cross-Polarization/Magic-Angle Spinning. Biomacromolecules 2005, 6, 468-474.

46. T Asakura,Y Suzuki, K Yazawa, A Aoki, Y Nishiyama, K Nishimura, F Suzuki, H Kaji, Determination of Accurate ^{1}H Positions of (Ala-Gly)n as a Sequential Peptide Model of *Bombyx Mori* Silk Fibroin before Spinning (Silk I). Macromolecules 2013, 46, 8046-8050.

47. Y Suzuki, T Yamazaki, A Aoki, H Shindo, T Asakura, NMR Study of the Structures of Repeated Sequences, GAGXGA (X = S, Y, V), in *Bombyx Mori* Liquid Silk. Biomacromolecules 2014, 15, 104-112

48. T Asakura, A Naito, Structure of silk I (*Bombyx mori* silk fibroin before spinning) in the dry and hydrated states studied using ^{13}C solid-state NMR spectroscopy. Int. J. Biol. Macromol. 2022, 216, 282-290.

49. T Asakura, J Yao, T Yamane, K Umemura, AS Ulrich, Heterogeneous Structure of Silk Fibers from *Bombyx Mori* Resolved by ^{13}C Solid-State NMR Spectroscopy. J. Am. Chem. Soc. 2002, 124, 8794-8795.

50. T Asakura, J Yao, ^{13}C CP/MAS NMR Study on Structural Heterogeneity in *Bombyx*

Mori Silk Fiber and Their Generation by Stretching. Protein Sci. 2009, 11, 2706-2713.

51. DJ Strydom, T Haylett, RH Stead, The Amino-Terminal Sequence of Silk Fibroin Peptide Cp - A Reinvestigation. Biochem. Biophys. Res. Commun. 1977, 79, 932-938.

52. H Saitô, I Ando, High-Resolution Solid-State NMR Studies of Synthetic and Biological Macromolecules. Ann. Rep. NMR Spectrosc. 1989, 21, 209-290.

53. S Spera, A Bax, Empirical Correlation between Protein Backbone Conformation and Cα and Cβ ^{13}C Nuclear Magnetic Resonance Chemical Shifts. J. Am. Chem. Soc. 1991, 113, 5490-5492.

54. M Iwadate, T Asakura, MP Williamson, Cα and Cβ Carbon-13 Chemical Shifts in Proteins From an Empirical Database. J. Biomol. NMR 1999, 13,199-211.

55. DS Wishart, Interpreting Protein Chemical Shift Data. Prog. Nucl. Magn.Reson. Spectrosc. 2011, 58, 62-87.

56. T Asakura, A Aoki, K Komatsu, C Ito, I Suzuki, A Naito, H Kaji, Lamellar Structure in Alanine–Glycine Copolypeptides Studied by Solid-State NMR Spectroscopy: A Model for the Crystalline Domain of *Bombyx Mori* Silk Fibroin in Silk II Form. Biomacromolecules 2020, 21, 3102-3111.

57. T Asakura, T Ogawa, A Naito, MP Williamson, Chain-Folded Lamellar Structure and Dynamics of the Crystalline Fraction of *Bombyx Mori* Silk Fibroin and of $(Ala\text{-}Gly\text{-}Ser\text{-}Gly\text{-}Ala\text{-}Gly)_n$ Model Peptides. Int. J. Biol. Macromol., 2020, 164, 3974-3983.

58. I Schnell, SP Brown, HY Low, H Ishida, HW Spiess, An Investigation of Hydrogen Bonding in Benzoxazine Dimers by Fast Magic-Angle Spinning and Double-Quantum ^{1}H NMR Spectroscopy. J. Am. Chem. Soc., 1998, 120, 11784-11795.

59. SP Brown, Application of high-resolution ^{1}H solid-state NMR. Solid State Nucl. Magn. Reson. 2012, 41, 1- 27 and references therein.

60. T Asakura, T Ohata, S Kametani, K Okushita, K Yazawa, Y Nishiyama, K Nishimura, A Aoki, F Suzuki, H Kaji, AS Ulrich, MP Williamson, Intermolecular

Packing in *B. Mori* Silk Fibroin: Multinuclear NMR Study of the Model Peptide (Ala-Gly)$_{15}$ Defines a Heterogeneous Antiparallel Antipolar Mode of Assembly in the Silk II Form. Macromolecules 2015, 48, 28-36.

61. T Asakura, Y Nakazawa, E Ohnishi, F Moro, Evidence from ^{13}C Solid-State NMR Spectroscopy for a Lamella Structure in an Alanine-Glycine Copolypeptide: A Model for the Crystalline Domain of *Bombyx Mori* Silk Fiber. Protein Sci. 2005, 14, 2654-2657.

62. T Asakura, H Sato, F Moro, Y Nakazawa, A Aoki, Lamellar Structure in Poly(Ala-Gly) Determined by Solid-State NMR and Statistical Mechanical Calculations. J. Am. Chem. Soc. 2007, 129, 5703-5709.

63. HT Edzes, JPC Bernards, Two-Dimensional Exchange NMR in Static Powders: Interchain ^{13}C Spin Exchange in Crystalline Polyethylene; J. Am.Chem. Soc.,1984, 106, 1515-1517.

64. PM Henrichs, M Linder, Carbon-13 Spin Diffusion in the Determination of Intermolecular Structure in Solids. J. Magn. Reson., 1984, 58, 458-461.

65. T Nakai, J Ashida, T Terao, Measurements of two-dimensional NMR powder patterns in rotations solids, J. Chem. Phys. 1988, 88, 6049-6058.

66. B Blumich, A Hagemeyer, Two-Dimensional ^{13}C Exchange Spectroscopy with Off-Magic Angle Spinning. *Chem.* Phys. Lett., 1989, 161, 55-59.

67. A Hagemeier, K Schmidt-Rohr, HW Spiess, Two-Dimensional Nuclear Magnetic Resonance Experiments for Studying Molecular Order and Dynamics in Static and in Rotating Solids, Adv. Magn. Reson., 1989, 13, 85-130.

68. J Ashida, D Kuwahara, T Uegaki, T Terao, Tensorial Interaction Correlation 2D Powder Patterns. Proceedings of the NMR Conference, Kyoto, 1990, p245-246.

69. Z Luz, HW Spiess, JJ Titman, Rotor-Synchronized MAS Two-Dimensional Exchange NMR in Solids. Principles and Applications, Israel J. Chem., 1992, 32, 145-160.

70. G Dabbagh, DP Weliky, R Tycko, Determination of Monomer Conformations in Noncrystalline Solid Polymers by Two-Dimensional NMR Exchange Spectroscopy. Macromolecules 1994, 27, 6183-6191.

71. R Tycko, DP Weliky, AE Berger, Investigation of Molecular Structure in Solids by Two-Dimensional NMR Exchange Spectroscopy with Magic Angle Spinning. J. Chem. Phys., 1996, 105, 7915-7930.

72. DP Weliky, R Tycko, Determination of Peptide Conformations by Two-Dimensional Magic Angle Spinning NMR Exchange Spectroscopy with Rotor Synchronization; J. Am. Chem. Soc., 1996, 118, 8487-8488.

73. J Kuemmerlen, JD van Beek, F Vollrath, BH Meier, Local structure in spider dragline silk investigated by 2D spin-diffusion NMR. Macromolecules, 1996, 29, 2920-2928.

74. P Robyr, M Utz, Z Gan, C Scheuer, M Tomaselli, UW Suter, R Ernst, Orientation of the Chemical Shielding Anisotropy Tensor of the Carbonate Carbon in Diphenyl Carbonate and Its Consequences for NMR studies on Polycarbonate. Macromolecules, 1998, 31, 5818-5822.

75. JD Van Beek, L Beaulieu, H Schäfer, M Demura, T Asakura, BH Meier, Secondary structure of a fibrous proteins : Solid-state NMR of silk from *Samia cynthia ricini*. Nature, 2000, 405,1077-1079.

76. J Ashida, K Ohgo, T Asakura, Determination of the Torsion Angles of Alanine and Glycine Residues of *Bombyx Mori* Silk Fibroin and the Model Peptides in the Silk I and Silk II Forms Using 2D Spin Diffusion Solid-State NMR under Off Magic Angle Spinning. J. Phys.Chem. B 2002, 106, 9434-9439.

77. J Ashida, K Ohgo, K Komatsu, A Kubota, T Asakura, Determination of the Torsion Angles of Alanine and Glycine Residues of Model Compounds of Spider Silk $(AGG)_{10}$ Using Solid-State NMR Methods. J. Biomol. NMR 2003, 25, 91-103.

78. T Gullion, J Schaefer, Detection of Weak Heteronuclear Dipolar Coupling by

Rotational-Echo Double-Resonance Nuclear Magnetic Resonance, Adv. Magn. Reson., 1989, 13, 57-83.

79. T Gullion, J Schaefer, Elimination of Resonance Offset Effects in Rotational-Echo, Double-Resonance NMR, J. Magn. Reson. 1991, 92, 439-442.

80. T Gullion, DB Baker, J Schaefer, New, Compensated Carr-Purcell Sequences, J. Magn. Reson. 1990, 89, 479-484.

81. CA Michal, LW Jelinski, Rotational-echo Double-resonance in Complex Biopolymers: a Study of *Nephila Clavipes* Dragline Silk J. Biomol. NMR 1998, 12, 231-241.

82. Y Suzuki, T Asakura, Local Conformation of Serine Residues in a Silk Model Peptide, $(Ala\text{-}Gly\text{-}Ser\text{-}Gly\text{-}Ala\text{-}Gly)_5$, Studied with Solid-State NMR:REDOR. Polym. J. 2010, 42, 354-356.

83. Y Suzuki, A Aoki, Y Nakazawa, DP Knight, T Asakura, Structural Analysis of the Synthetic Peptide $(Ala\text{-}Gly\text{-}Ser\text{-}Gly\text{-}Ala\text{-}Gly)_5$, a Model for the Crystalline Domain of *Bombyx Mori* Silk Fibroin, Studied with ^{13}C CP/MAS NMR, REDOR, and Statistical Mechanical Calculations. Macromolecules 2010, 43, 9434-9440.

84. KP McGrath, MJ Fournier, TL Mason, DA Tirrell, Genetically directed syntheses of new polymeric materials. Expression of artificial genes encoding proteins with repeating-$(AlaGly)_3ProGluGly$-elements. J. Am. Chem. Soc. 1992, 114, 727-733.

85. A Parkhe, MJ Fournier, TL Mason, DA Tirrell, Determination of the chain-folding pattern in the crystalline domains of the repetitive polypeptide $\{(AlaGly)_3GluGly(GlyAla)_3GluGly\}_{10}$ by FTIR studies of its blends with a carbon-13 enriched analog. Macromolecules 1993, 26, 6691-6693.

86. MT Krejchi, EDT Atkins, AJ Waddon, MJ Fournier, TL Mason, DA Tirrell, Chemical Sequence Control of β-Sheet Assembly in Macromolecular Crystals of Periodic Polypeptides. Science 1994, 265, 1427-1432.

87. A Keller, A note on single crystals in polymers: Evidence for a folded chain configuration. The Philosophical Magazine: A Journal of Theoretical Experimental and Applied Physics 1957, 2, 1171-1175.

88. A Panitch, K Matsuki, EJ Cantor, SJ Cooper, EDT Atkins, MJ Fournier, TL Mason, DA Tirrell, Poly(LAlanylglycine): Multigram-Scale Biosynthesis, Crystallization, and Structural Analysis of Chain-Folded Lamellae. Macromolecules 1997, 30, 42-49.

89. RDB Fraser, TP MacRae, FHC Stewart, Poly-L-alanylglycyl-L-alanyl- glycyl-L-serylglycine: a model for the crystalline regions of silk fibroin. J. Mol. Biol. 1966, 19, 580-582.

90. RDB Fraser, TP MacRae, FHC Stewart, E Suzuki, Poly-L-alanylglycine. J. Mol. Biol. 1965, 11, 706-712.

91. MT Krejchi, SJ Cooper, Y Deguchi, EDT Atkins, MJ Fournier, TL Mason, DA Tirrell, Crystal Structures of Chain-Folded Antiparallel β-Sheet Assemblies from Sequence-Designed Periodic Polypeptides. Macromolecules 1997, 30, 5012-5024.

92. H Saito, R Tabeta, A Kuzuhara, T Asakura, A ^{2}H NMR Study of [Ser-3,3-$^{2}H_2$]- and [Ala-3,3,3,-$^{2}H_3$]-Silk Fibroins in the Solid State. Role of Side-Chain Moiety in Stabilization of Secondary Structure. Bull. Chem. Soc. Jpn. 1986, 59, 3383-3387.

93. T Asakura, M Minami, R Shimada, M Demura, M Osanai, T Fujito, M Imanari, AS Ulrich, ^{2}H-Labeling of Silk Fibroin Fibers and Their Structural Characterization by Solid-State ^{2}H NMR. Macromolecules 1997, 30, 2429-2435.

94. K Takegoshi, S Nakamura, T Terao, ^{13}C−^{1}H dipolar-assisted rotational resonance in magic-angle-spinning NMR. Chem. Phys. Lett. 2001, 344, 631−637.

95. K Takegoshi, S Nakamura, T Terao, ^{13}C−^{1}H dipolar driven ^{13}C−^{13}C recoupling without ^{13}C RF irradiation in nuclear magnetic resonance of rotating solids. J. Chem. Phys. 2003, 118, 2325−2341.

96. MJ Bayro, M Huber, R Ramachandran, TC Davenport, BH Meier, M Ernst, RG

Griffin, Dipolar truncation in magic angle spinning NMR recoupling experiments. J. Chem. Phys. 2009, 130,114506.

97. GP Holland, MS Creager, JE Jenkins, RV Lewis, JL Yarger, Determining Secondary Structure in Spider Dragline Silk by Carbon−Carbon Correlation Solid-State NMR Spectroscopy. J. Am. Chem. Soc. 2008, 130, 9871−9877.

98. JE Jenkins, MS Creager, RV Lewis, GP Holland, JL Yarger, Quantitative correlation between the protein primary sequences and secondary structures in spider dragline silks. Biomacromolecules 2010, 11, 192−200.

99. T Izdebski, P Akhenblit, JE Jenkins, JL Yarger, GP Holland, Structure and Dynamics of Aromatic Residues in Spider Silk: 2D Carbon Correlation NMR of Dragline Fibers. Biomacromolecules 2010,11, 168−174.

100. JE Jenkins, GP Holland, JL Yarger, Characterizing the Secondary Protein Structure of Black Widow Dragline Silk Using Solid-State NMR and X-ray Diffraction. Biomacromolecules 2013, 14, 3472−3483.

101. T Asakura, A Nishimura, S Kametani, S Kawanishi, A Aoki, F Suzuki, H Kaji, A Naito, Refined Crystal Structure of *Samia cynthia ricini* Silk Fibroin Revealed by Solid-State NMR Investigations. Biomacromolecules 2017, 18, 1965−1974.

102. A Naito, K Okushita, K Nishimura, GS Boutis, A Aoki, T Asakura, Quantitative Analysis of Solid-State Homonuclear Correlation Spectra of Antiparallel β-Sheet Alanine Tetramers. J. Phys. Chem. B. 2018, 122, 2715-2724.

103. K Okushita, A Asano, MP Williamson, T Asakura, Local Structure and Dynamics of Serine in the Heterogeneous Structure of the Crystalline Domain of Bombyx mori Silk Fibroin in Silk II Form Studied by 2D $^{13}C-^{13}C$ Homonuclear Correlation NMR and Relaxation Time Observation. Macromolecules 2014, 47, 4308−4316.

104. T Asakura, M Iwadate, M Demura, MP Williamson, Structural Analysis of Silk with ^{13}C NMR Chemical Shift Contour Plots. Int. J. Biol. Macromol. 1999, 4,167-171.

105. T Asakura, Y Watanabe, A Uchida, H Minagawa, NMR of Silk fibroin.2. ^{13}C NMR Study of the Chain Dynamics and Solution Structure of *Bombyx Mori* Silk Fibroin. Macromolecules 1984**,** 17, 1075-1081.

106. DA Torchia, The measurement of proton-enhanced carbon-13 T_1 values by a method which suppresses artifacts. J. Magn. Reson. 1978, 30, 613-616.

107. H Saito, M Ishida, M Yokoi, T Asakura, Dynamic Features of Side Chains in Tyrosine and Serine Residues of Some Polypeptides and Fibroins in the Solid as Studied by High-Resolution Solid-State ^{13}C NMR Spectroscopy. Macromolecules 1990, 23, 83-88.

108. T Kameda, Y Ohkawa, K Yoshizawa, J Naito, AS Ulrich, T Asakura, Hydrogen-Bonding Structure of Serine Side Chains in *Bombyx Mori* and *Samia Cynthi Ricini* Silk Fibroin Determined by Solid-State ^{2}H NMR. Macromolecules 1999, 32, 7166-7171.

109. T Asakura, R Sugino, J Yao, H Takashima, R Kishore, Comparative Structure Analysis of Tyrosine and Valine Residues in Unprocessed Silk Fibroin (Silk I) and in the Processed Silk Fiber (Silk II) from *Bombyx Mori* Using Solid-State ^{13}C, ^{15}N, and ^{2}H NMR. Biochemistry 2002, 41, 4415–4424.

110. T Asakura, R Sakaguchi, M Demura, T Manabe, A Uyama, K Ogawa, M Osanai, In Vitro Production of *Bombyx Mori* Silk Fibroin by Organ Culture of the Posterior Silk Glands; Isotope Labeling and Fluorination of the Silk Fibroin. Biotechnol. Bioeng. 1993, 41, 245–252.

111. LK Nicholson, T Asakura, M Demura, TA Cross, A Method for Studying the Structure of Uniaxially Aligned Biopolymers Using Solid State ^{15}N-NMR: Application to *Bombyx Mori* Silk Fibroin Fibers. Biopolymers 1993, 33, 847–861.

112. T Asakura, Y Sato, A Aoki, Stretching-Induced Conformational Transition of the Crystalline and Noncrystalline Domains of ^{13}C-Labeled *Bombyx Mori* Silk Fibroin Monitored by Solid State NMR. Macromolecules 2015, 48, 5761–5769.

113. T Asakura, K Suita, T Kameda, S Afonin, AS Ulrich, Structural Role of Tyrosine in *Bombyx Mori* Silk Fibroin, Studied by Solid-State NMR and Molecular Mechanics

on a Model Peptide Prepared as Silk I and II. Magn. Reson. Chem. 2004, 42, 258–266.

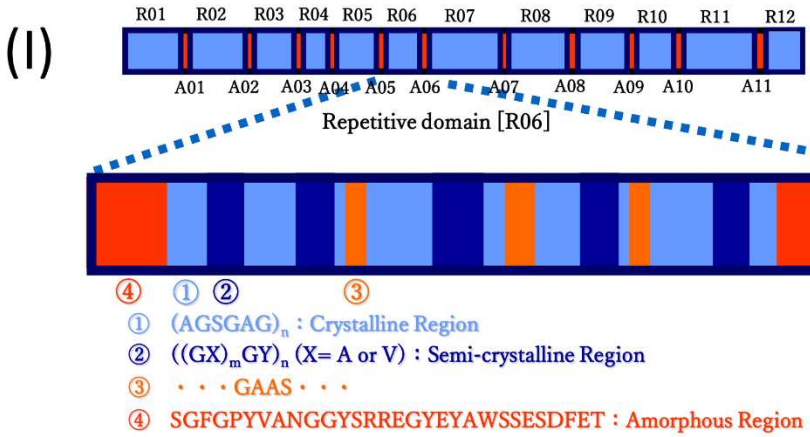

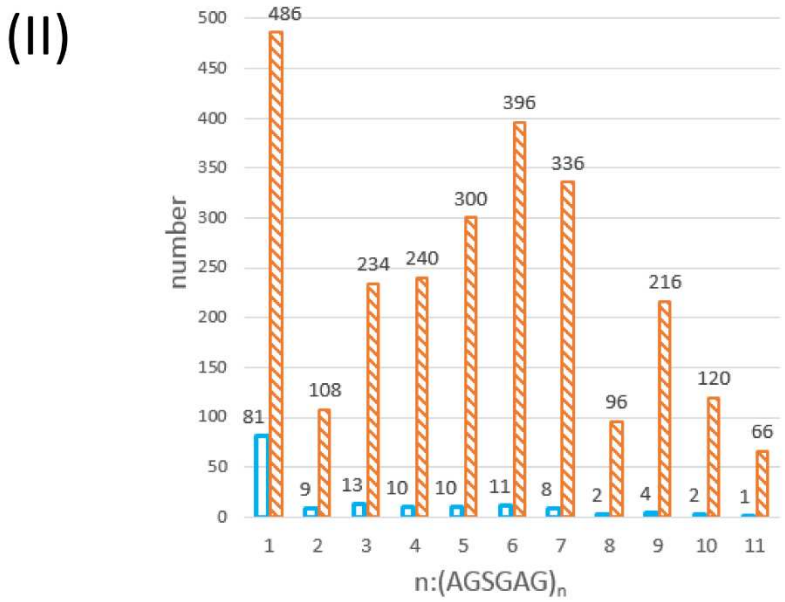

Figure 1. (I) The organization of the *B. mori* silk fibroin heavy chain gene. R01····R12 and A01····A11 represent the predicted twelve repetitive and eleven amorphous regions, respectively, in the polypeptide chain.[32,33] An approximate amino acid sequence of the R06 region is illustrated by sequences ① - ④. Adapted with permission from Asakura et al., Possible Implications of Serine and Tyrosine Residues and Intermolecular Interactions on the Appearance of Silk I Structure of *Bombyx Mori* Silk Fibroin-Derived Synthetic Peptides: High-Resolution ^{13}C Cross-Polarization/Magic-Angle Spinning. Biomacromolecules 2005, 6, 468-474. Copyright 2005 American Chemical Society. (II) Histograms of the number of occurrences of each $(AGSGAG)_n$ sequence for n=1–11 (blue), and the total number of amino acid residues of each $(AGSGAG)_n$ sequence in the primary structure of SF heavy chain (orange stripes). Reprinted from Int. J. Biol. Macromol., 164, 3974-3983, Asakura et al., Chain-Folded Lamellar Structure and Dynamics of the Crystalline Fraction of *Bombyx Mori* Silk Fibroin and of $(Ala\text{-}Gly\text{-}Ser\text{-}Gly\text{-}Ala\text{-}Gly)_n$ Model Peptides. Int. J. Biol. Macromol., Copyright (2020), with permission from Elsevier.

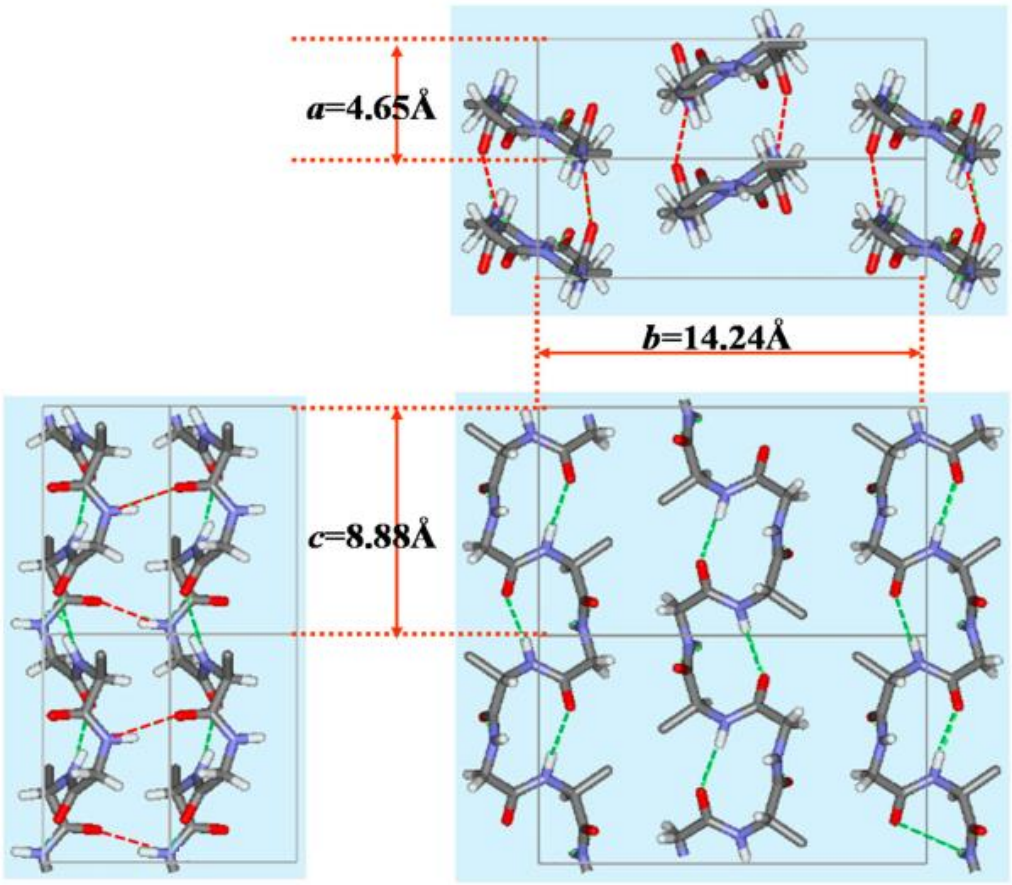

Figure 2. Packing structure of poly(AG) chains with type II β-turn structure as a model for Silk I*, shown in three orthogonal directions.[28] Dotted lines denote intra- (green) and inter- (red) molecular hydrogen bonds. The unit lattice values ***a***, ***b*** and ***c*** were obtained from X-ray diffraction data. Adapted with permission from Asakura et al., Refinement of Repeated β-Turn Structure for Silk I Conformation of *Bombyx Mori* Silk Fibroin Using ^{13}C Solid-State NMR and X-Ray Diffraction Methods. Macromolecules 2005, 38, 7397-7403. Copyright 2005 American Chemical Society.

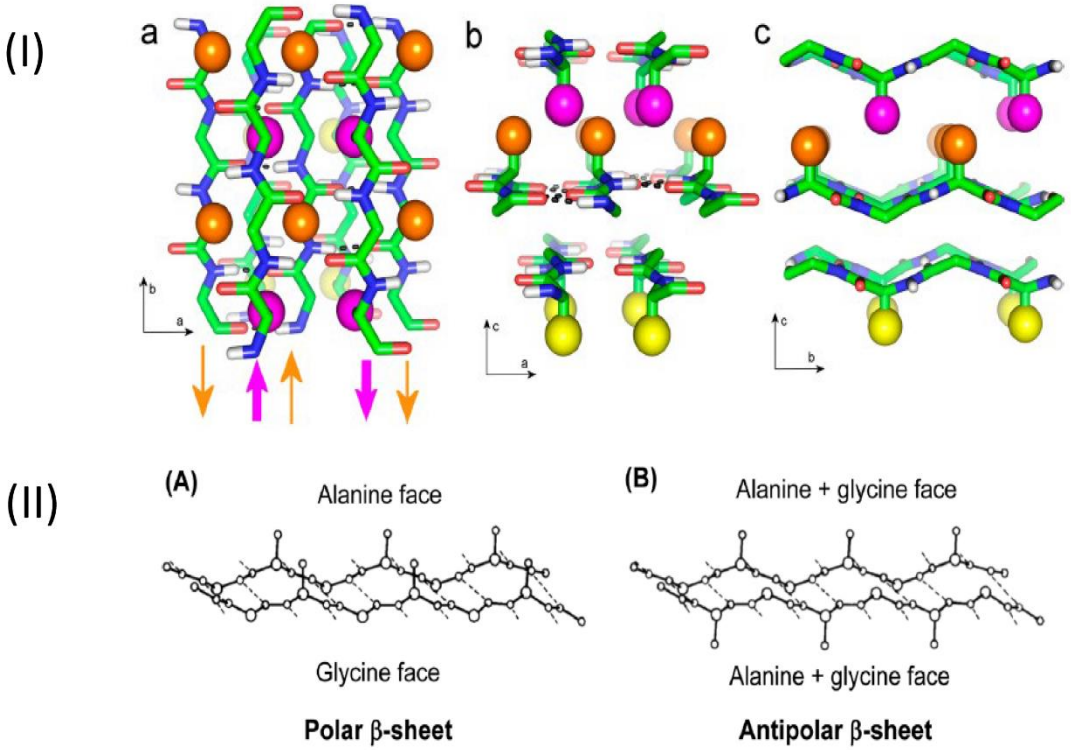

Figure 3. (I) Marsh model of poly(AG).[19] The model is shown in three orthogonal orientations, with the relevant unit cell axes shown. Three β-sheet layers are shown. In the top layer, methyl groups are in magenta; in the middle layer they are in orange; and in the bottom layer they are in yellow. Interstrand hydrogen bonds are indicated for the central sheet. The directions of the strands are shown beneath panel (a), with the top strand in magenta and the central strand in orange. Adapted with permission from Asakura et al., Intermolecular Packing in *B. Mori* Silk Fibroin: Multinuclear NMR Study of the Model Peptide $(Ala\text{-}Gly)_{15}$ Defines a Heterogeneous Antiparallel Antipolar Mode of Assembly in the Silk II Form. Macromolecules 2015, 48, 28-36. Copyright 2015 American Chemical Society. (II) Schematic illustration of (A) polar and (B) antipolar poly(AG) β-sheets obtained by conformational energy calculations. The polar β-sheet has an Ala face and a Gly face, while the antipolar β-sheet has two identical faces.[22] Reprinted with permission from Fossey et al., Conformational Energy Studies of β-Sheets of Model Silk Fibroin Peptides. I. Sheets of Poly(Ala-Gly) Chains. Biopolymers 1991, 31,1529−1541. Copyright 1991 John Wiley and Sons.

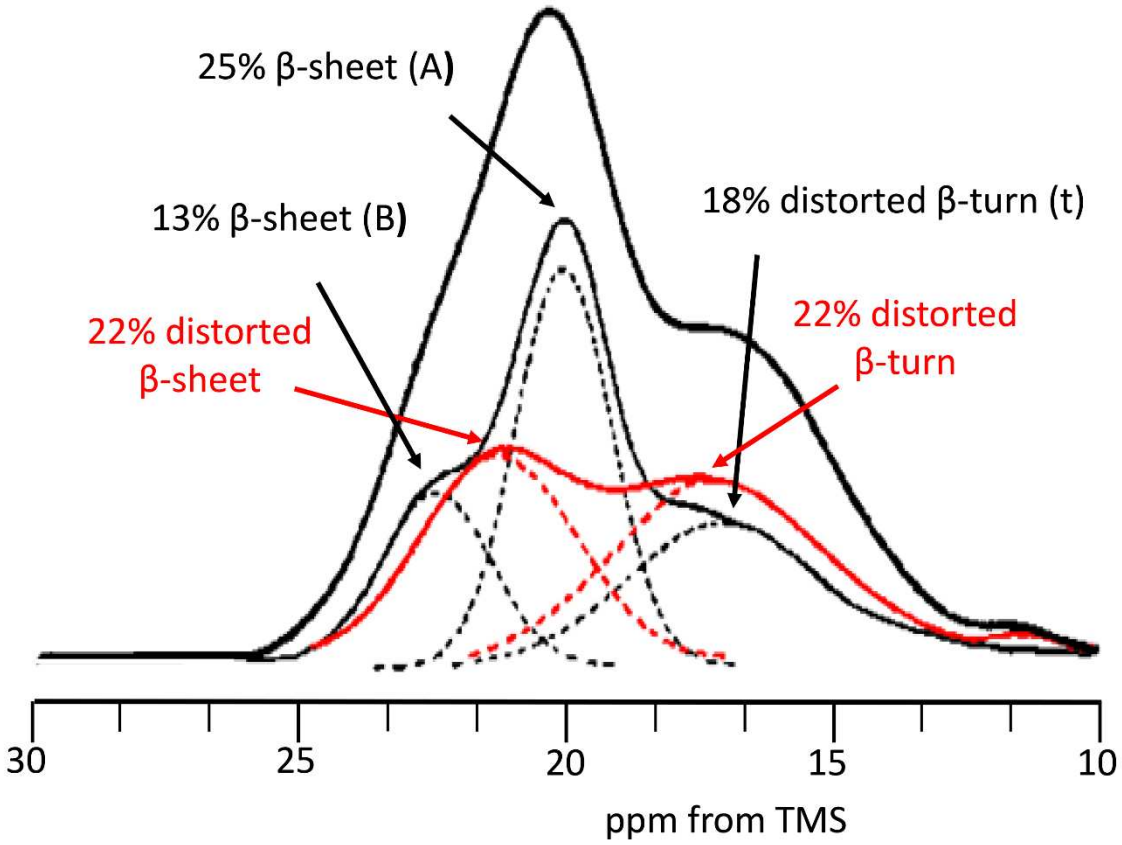

Figure 4. Expanded Ala Cβ peak from the ^{13}C solid-state NMR spectrum of [3-^{13}C]Ala silk fibroin fiber (thick solid, black) with the assignment of each component. The crystalline domain (56% ; thin solid, black) with the sequence $(AGSGAG)_n$ consists of 18% distorted β-turns (t), 25% β-sheet (A), and 13% β-sheet (B). The non-crystalline domain (44%, red) consists of 22% distorted β-turns and 22% distorted β-sheets. Adapted with permission from Asakura et al., Heterogeneous Structure of Silk Fibers from *Bombyx Mori* Resolved by ^{13}C Solid-State NMR Spectroscopy. J. Am. Chem. Soc. 2002, 124, 8794-8795. Copyright 2002 American Chemical Society.

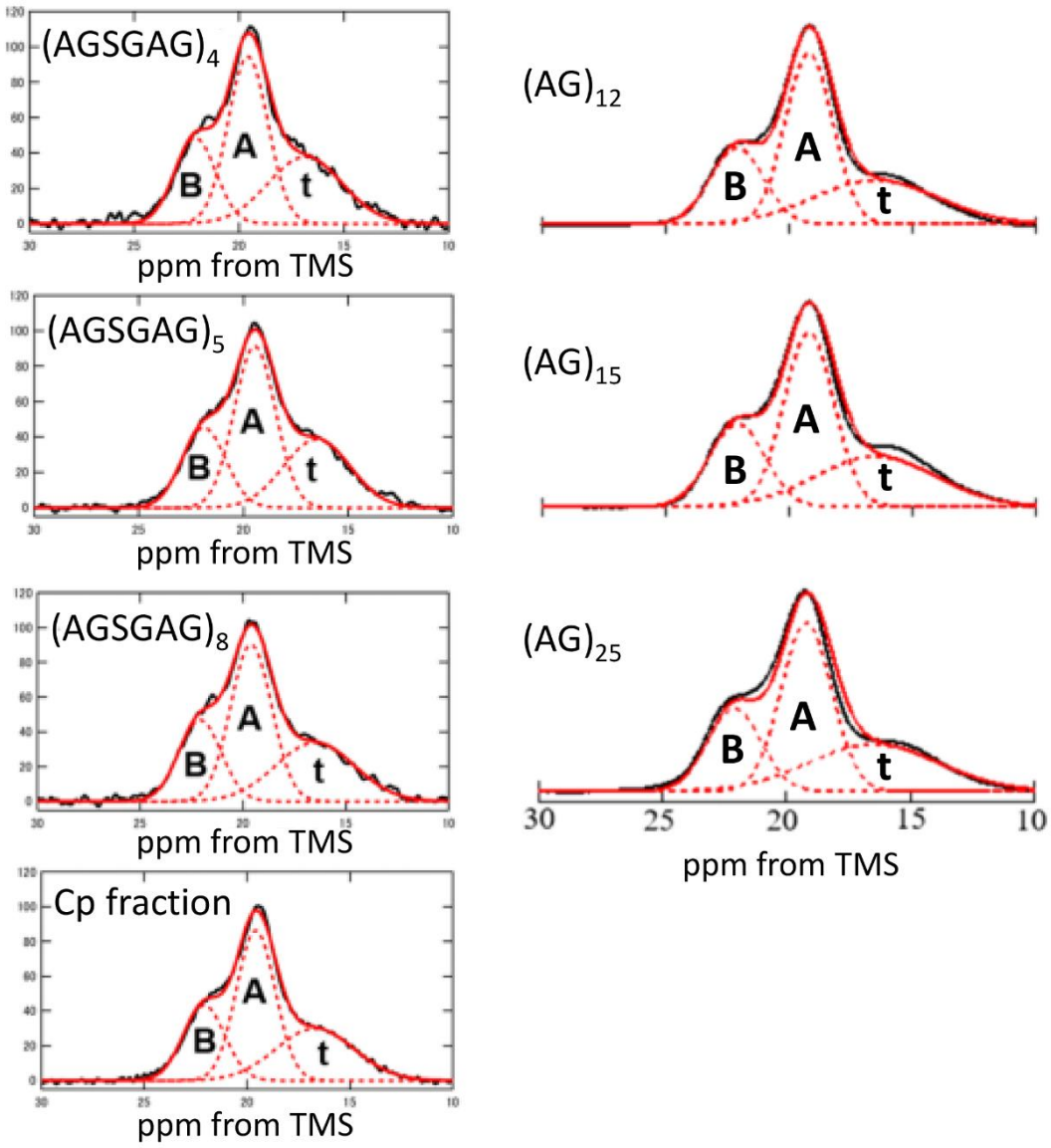

Figure 5. ^{13}C CP/MAS NMR spectra of the Ala Cβ peaks from different peptides (black), showing deconvolutions into three components: **t** (distorted β-turn), and two different antiparallel β-sheet signals **A** and **B**. Left panels adapted from Int. J. Biol. Macromol., 164, 3974-3983, Asakura et al., Chain-Folded Lamellar Structure and Dynamics of the Crystalline Fraction of *Bombyx Mori* Silk Fibroin and of (Ala-Gly-Ser-Gly-Ala-Gly)$_n$ Model Peptides. Int. J. Biol. Macromol., Copyright (2020), with permission from Elsevier. Right panels adapted with permission from Asakura et al., Lamellar Structure in Alanine–Glycine Copolypeptides Studied by Solid-State NMR Spectroscopy: A Model for the Crystalline Domain of *Bombyx Mori* Silk Fibroin in Silk II Form. Biomacromolecules 2020, 21, 3102-3111. Copyright 2020 American Chemical Society.

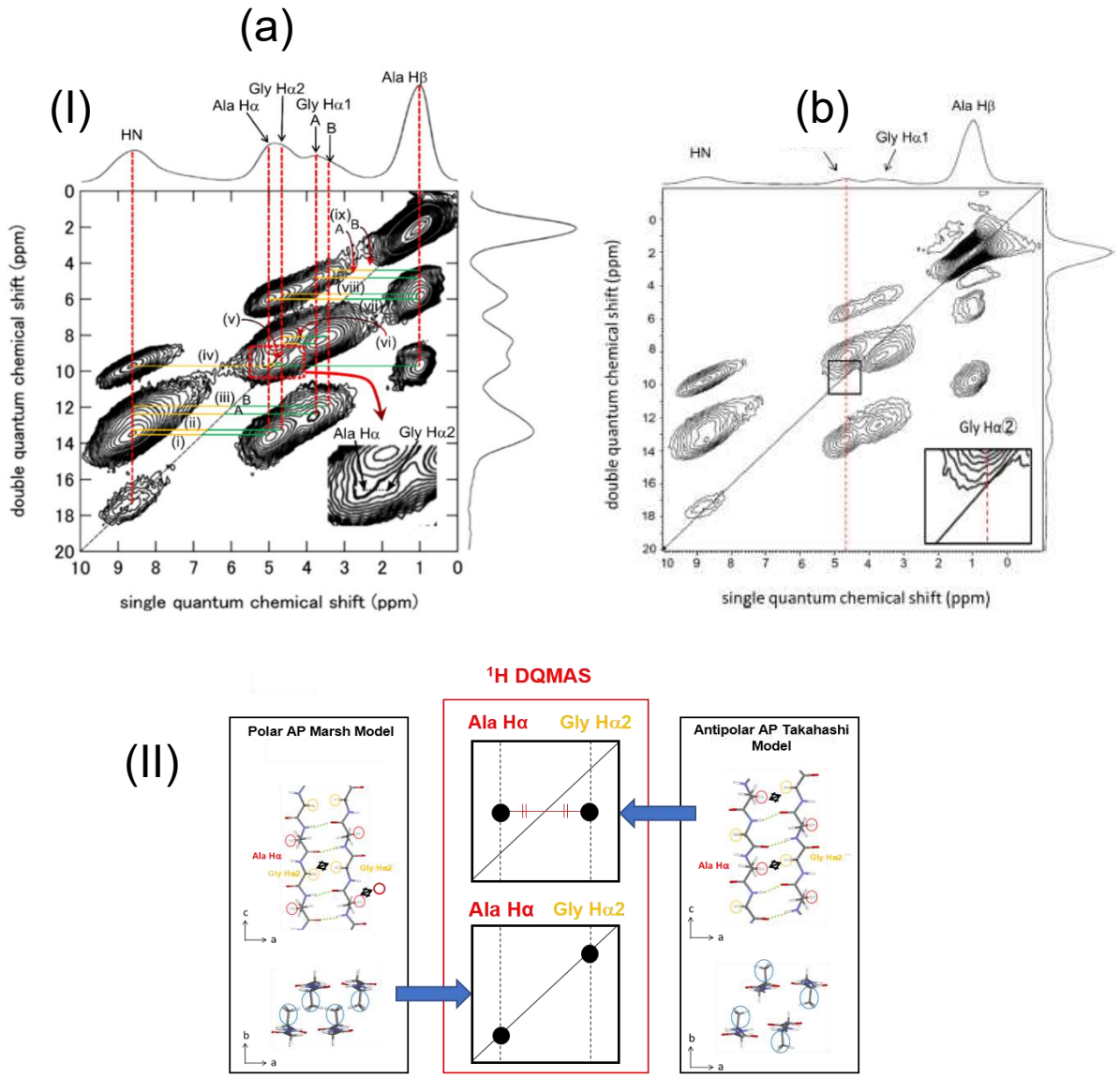

Figure 6. (I) (a) ^{1}H DQMAS spectrum of $(AG)_{15}$ in the Silk II form. Cross peaks are assigned as (i) AlaHα-AlaHN, (ii) GlyHα2-GlyHN, (iii) GlyHα1-GlyHN, (iv) AlaHβ-AlaHN, (v) AlaHα-GlyHα2, (vi) GlyHα2-GlyHα1, (vii) AlaHα-AlaHβ, (viii) GlyHα2-AlaHβ, (ix) GlyHα1-AlaHβ. (b) ^{1}H DQMAS spectrum of deuterium-labeled $([2\text{-}d_1]AG)_{15}$ in the Silk II form to remove spectral overlap in the Hα region (cf. Figure 6(I)). It is clear that there are no Gly Hα2−Gly Hα2 peaks on the diagonal. Adapted with permission from Asakura et al., Intermolecular Packing in *B. Mori* Silk Fibroin: Multinuclear NMR Study of the Model Peptide $(Ala\text{-}Gly)_{15}$ Defines a Heterogeneous Antiparallel Antipolar Mode of Assembly in the Silk II Form. Macromolecules 2015, 48, 28-36. Copyright 2015 American Chemical Society. (II) In the polar Marsh model,[19] the Gly $Hα_2$ protons in adjacent β-strands are about 2 Å apart, so a diagonal peak for Gly $Hα_2$ is expected. However, in the antipolar Takahashi model,[23] the $^{1}H–^{1}H$ distances between two Gly $Hα_2$ protons in adjacent β- strands are more than 4 Å, so a diagonal peak for Gly $Hα_2$ is not expected. On the other hand, the $^{1}H–^{1}H$ distances between Gly $Hα_2$ and Ala Hα are longer than 4 Å in the polar model, but about 2.4 Å in the antipolar model. Therefore, a cross peak should be observed in the antipolar model, but should not be observed in the polar model. Thus, $^{1}H–^{1}H$ distance information obtained from DQMAS ^{1}H NMR gives a clear conclusion about the packing of the AP β-sheet.

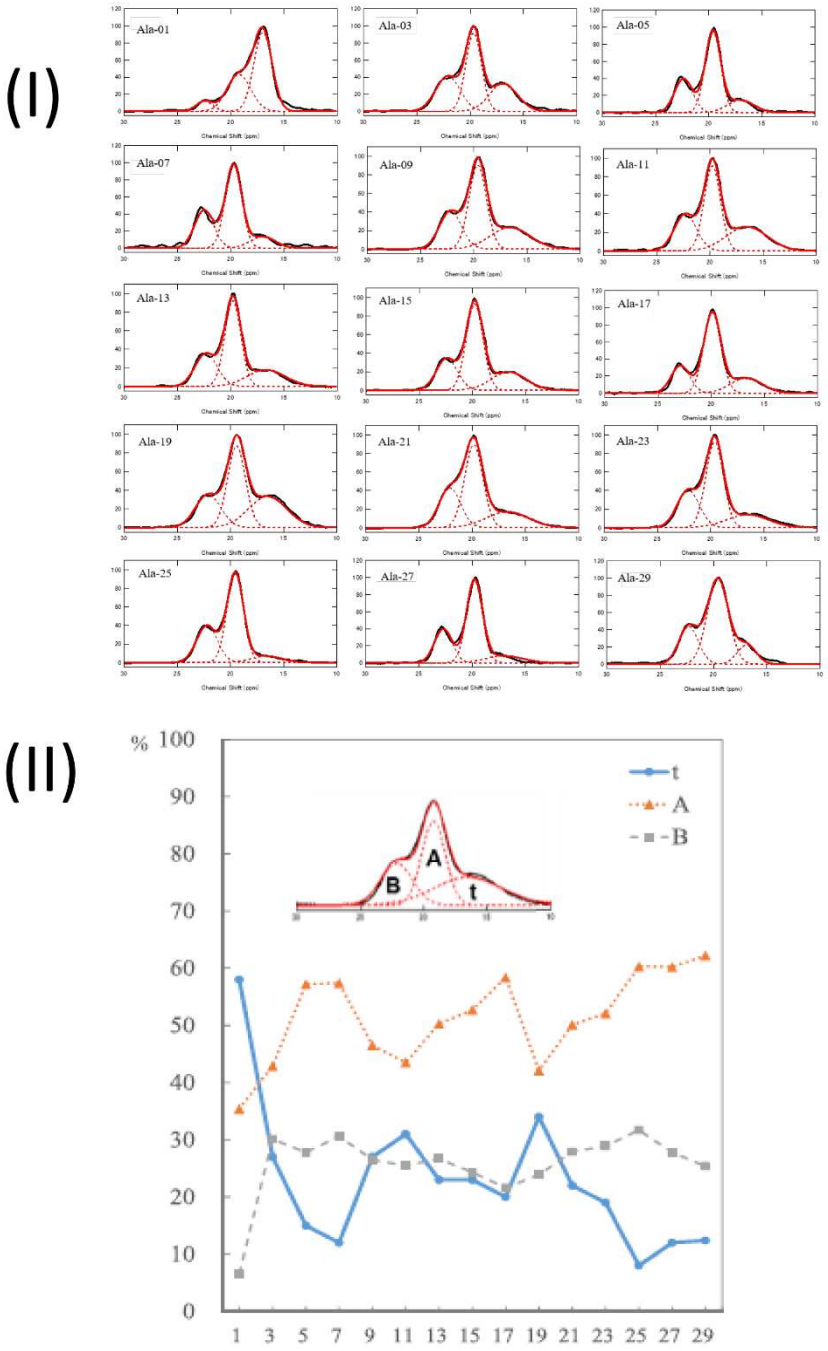

Figure 7. (I) Deconvoluted ^{13}C-labeled Ala Cβ peaks in the ^{13}C CP/MAS NMR spectra of all fifteen specifically [3-^{13}C]Ala-labeled $(AG)_{15}$ peptides. (II) Change in the fractions of **t**, **A**, and **B** of ^{13}C-labeled Ala Cβ peaks of 15 [3-^{13}C]Ala-$(AG)_{15}$ peptides plotted as a function of the ^{13}C-labeled site. Adapted with permission from Asakura et al., Lamellar Structure in Alanine–Glycine Copolypeptides Studied by Solid-State NMR Spectroscopy: A Model for the Crystalline Domain of *Bombyx Mori* Silk Fibroin in Silk II Form. Biomacromolecules 2020, 21, 3102-3111. Copyright 2020 American Chemical Society.

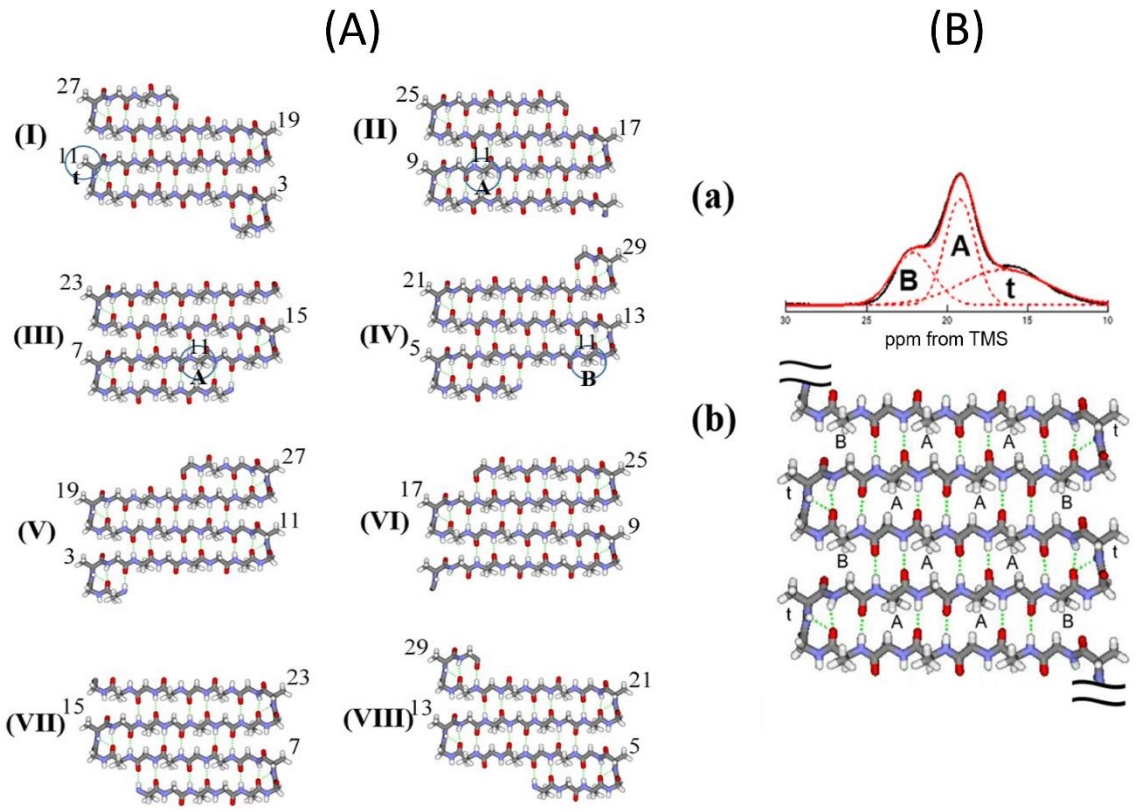

Figure 8. (A) Eight possible lamellar structures of $(AG)_{15}$, (I)-(VIII), derived by modelling repetitive folding through β-turns every eighth amino acid in an antipolar arrangement, with β-turns at all possible positions. Ala^{11} is marked by a circle in structures (I)-(IV). (B) (a) Assignment of Ala Cβ peaks deconvoluted to three peaks, i.e., two β-sheet signals, **A** and **B**, and one β-turn **t**, of $(AG)_m$ in the Silk II form. (b) Three peaks, **A**, **B** and **t**, can be assigned to three kinds of Ala Cβ carbons, **A**, **B** and **t** in the lamellar structure. Adapted with permission from Asakura et al., Lamellar Structure in Alanine–Glycine Copolypeptides Studied by Solid-State NMR Spectroscopy: A Model for the Crystalline Domain of *Bombyx Mori* Silk Fibroin in Silk II Form. Biomacromolecules 2020, 21, 3102-3111. Copyright 2020 American Chemical Society.

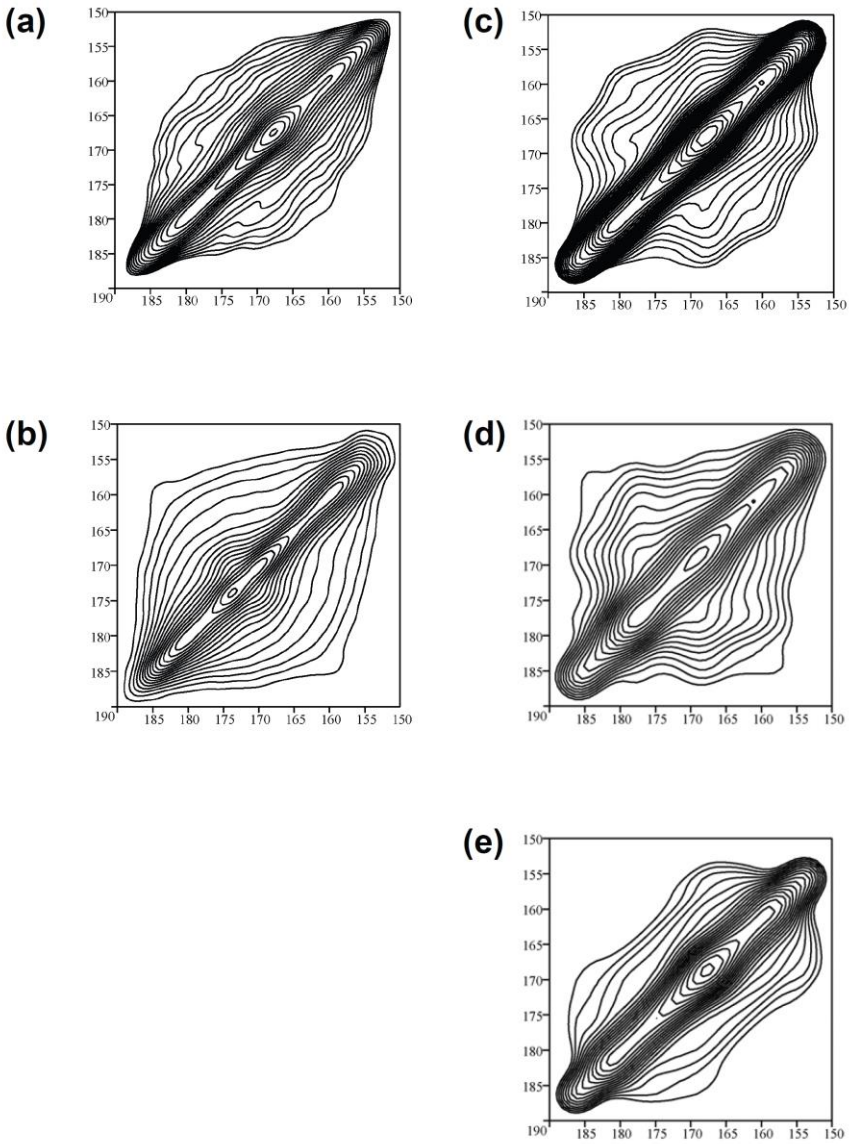

Figure 9. Expansion of the carbonyl region from ^{13}C spin diffusion NMR spectra of (a) $(AG)_6A[1\text{-}^{13}C]G^{14}[1\text{-}^{13}C]A^{15}G(AG)_7$ and (b)$(AG)_8A[1\text{-}^{13}C]G^{18}[1\text{-}^{13}C]A^{19}G(AG)_5$, observed under slow MAS condition. The corresponding simulated spectra, (c) and (d), and (e) the calculated spectrum for antiparallel β-sheet sheet, (modelled with $\phi = -150°$ and $\varphi = 150°$) are also shown. Adapted with permission from Asakura et al., Lamellar Structure in Poly(Ala-Gly) Determined by Solid-State NMR and Statistical Mechanical Calculations. J. Am. Chem. Soc. 2007, 129, 5703-5709. Copyright 2007 American Chemical Society.

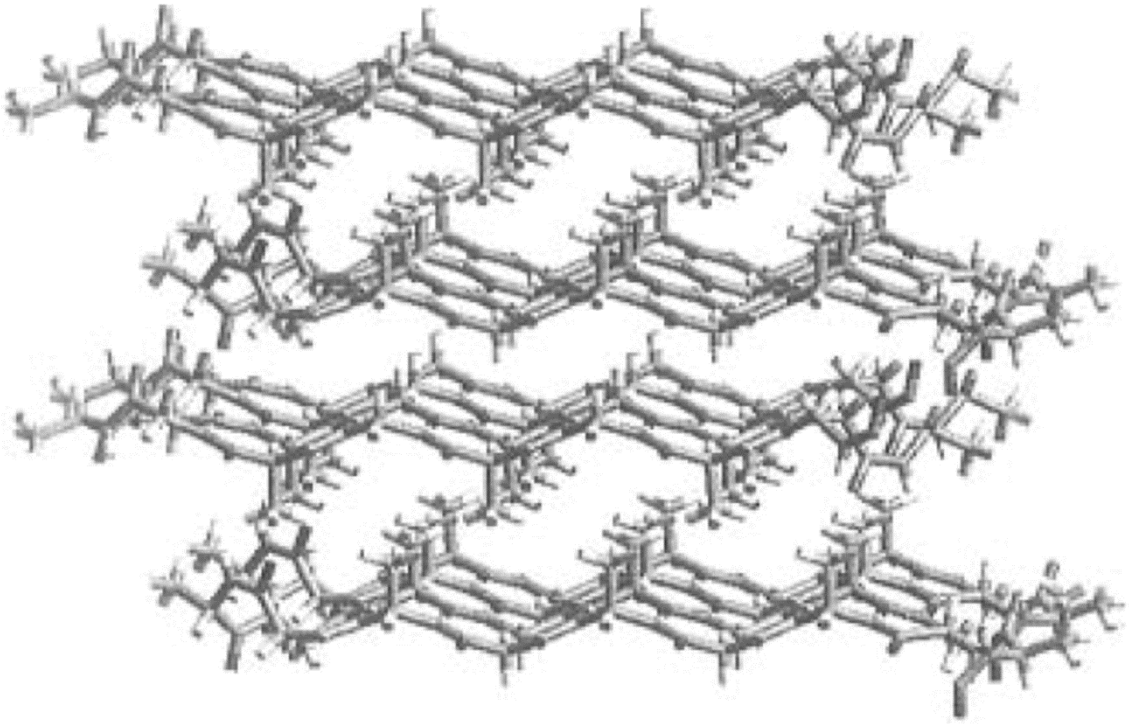

Figure 10. Three-dimensional structure of a stack of polar antiparalell β-sheets of poly(AG), folding in phase with an octapeptide periodicity and forming γ-turns. In the process of the preparation, various structures for poly(AG) were computer generated and the closest overall fit structure with the observed X-ray data is shown.
Adapted with permission from A Panitch et al., Poly(LAlanylglycine): Multigram-Scale Biosynthesis, Crystallization, and Structural Analysis of Chain-Folded Lamellae. Macromolecules 1997, 30, 42-49. Copyright (1997)American Chemical Society.

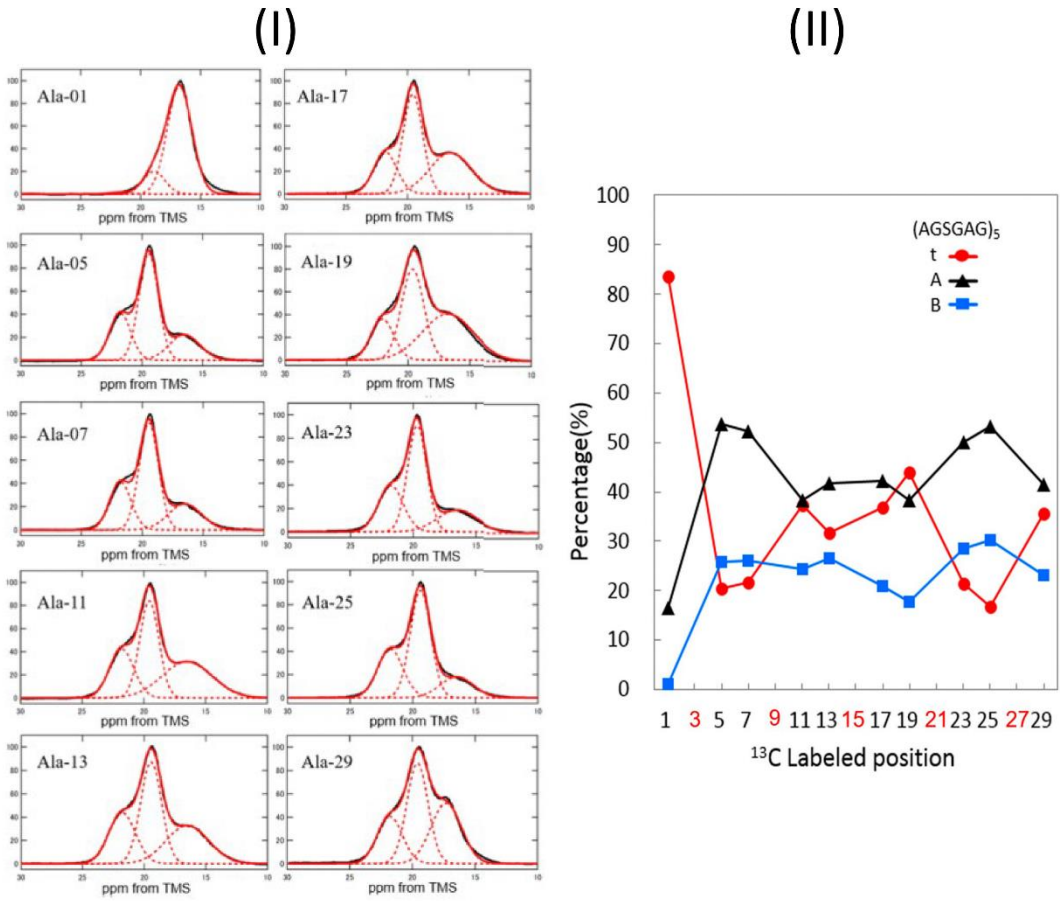

Figure 11. (I) Expanded ^{13}C-labeled Ala Cβ peaks in the ^{13}C CP/MAS NMR spectra of all ten individually [3-^{13}C]Ala-labeled $(AGSGAG)_5$ peptides. The three deconvoluted Ala Cβ peaks are assigned to **t** (distorted β-turn), **A** and **B** (center and end of antiparallel-β sheet respectively) of $(AGSGAG)_5$ as shown in Figure 4. (II) Changes in the percentages of peaks **t**, **A** and **B** of ^{13}C-labeled Ala Cβ carbon of all ten [3-^{13}C]Ala-$(AGSGAG)_5$ peptides plotted as a function of the ^{13}C-labeled position. The positions 3, 9, 15, 21 and 27 (red) in [3-^{13}C]Ala-$(AGSGAG)_5$ are Ser residues, not Ala. Reprinted from Int. J. Biol. Macromol., 164, 3974-3983, Asakura et al., Chain-Folded Lamellar Structure and Dynamics of the Crystalline Fraction of *Bombyx Mori* Silk Fibroin and of $(Ala\text{-}Gly\text{-}Ser\text{-}Gly\text{-}Ala\text{-}Gly)_n$ Model Peptides. Int. J. Biol. Macromol., Copyright (2020), with permission from Elsevier.

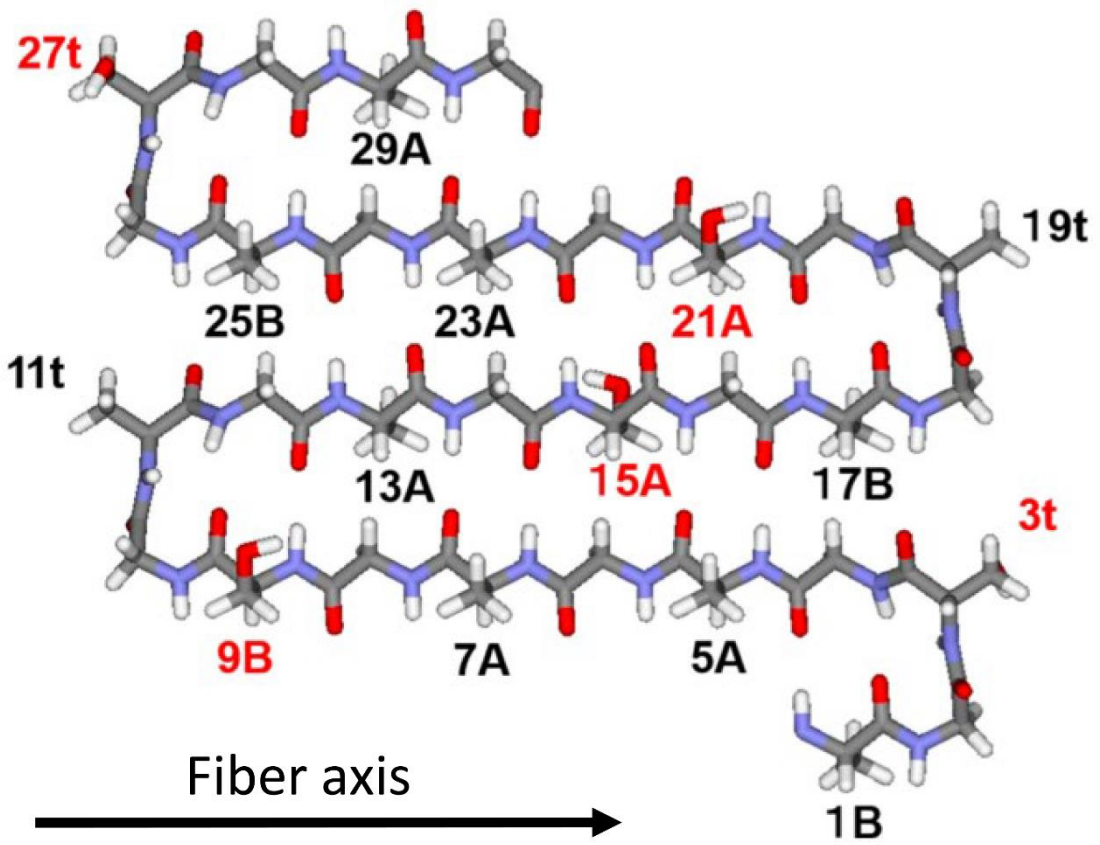

Figure 12. Lamellar structure of $(AGSGAG)_5$ in an antipolar arrangement with β-turns at positions 11 and 19, formed by repetitive folding using β-turns every eighth amino acid. Three peaks, **t**, **A** and **B** in the ^{13}C-labeled Ala Cβ peak can be assigned to three kinds of Ala Cβ carbons (black letters). The difference between **A** and **B** is that **B** is at the end of the β-strand whereas **A** is in the middle of the strand. The red letters indicate the Ser Cβ carbons in $(AGSGAG)_5$ corresponding to the Ala Cβ carbons in $(AG)_{15}$ lamellar structure. The side chain conformations of the Ser Cα-Cβ bonds were modelled as gauche+. The Cα-$^2H_2$ bond of Gly and the Cα-Cβ^2H_3 bond of Ala are perpendicular to the fiber axis. Reprinted from Int. J. Biol. Macromol., 164, 3974-3983, Asakura et al., Chain-Folded Lamellar Structure and Dynamics of the Crystalline Fraction of *Bombyx Mori* Silk Fibroin and of $(Ala\text{-}Gly\text{-}Ser\text{-}Gly\text{-}Ala\text{-}Gly)_n$ Model Peptides. Int. J. Biol. Macromol., Copyright (2020), with permission from Elsevier.

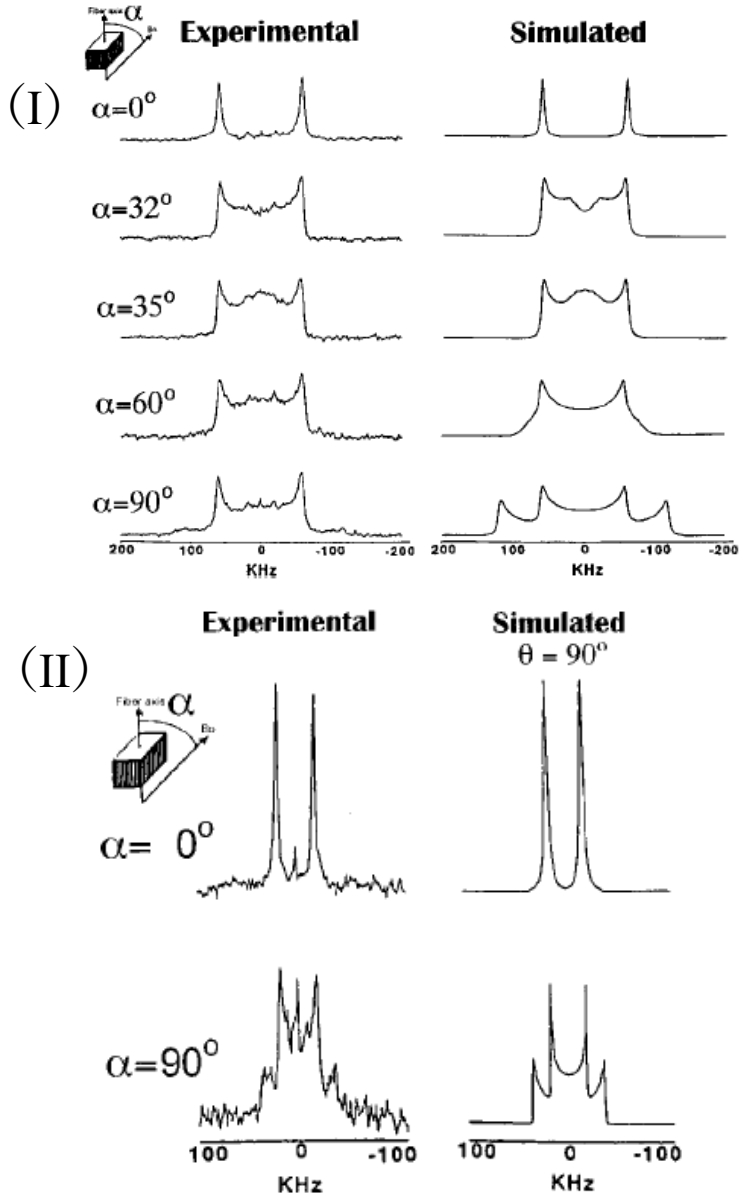

Figure 13. Experimental and simulated ^{2}H solid-state NMR spectra of uniaxially aligned (I) [2,2-$^{2}H_2$]Gly- and (II) [3,3,3-$^{2}H_3$]Ala-SF fibers.The angle α between the fiber axis and magnetic field was set to be (I) 0°, 32°, 35°,60° and 90°, and (II) 0° and 90°. When the angle between the Cα-$^{2}H_2$ bond of Gly and fiber axis was assumed to be 90°, the experimental spectra could be well simulated as shown in (I). Similarly, a good agreement was also obtained when the angle between the Cα-Cβ$^{2}H_3$ bond of Ala and the fiber axis was assumed to be 90° for (II). Adapted with permission from Asakura et al., ^{2}H-Labeling of Silk Fibroin Fibers and Their Structural Characterization by Solid-State ^{2}H NMR. Macromolecules 1997, 30, 2429-2435. Copyright 1997 American Chemical Society.

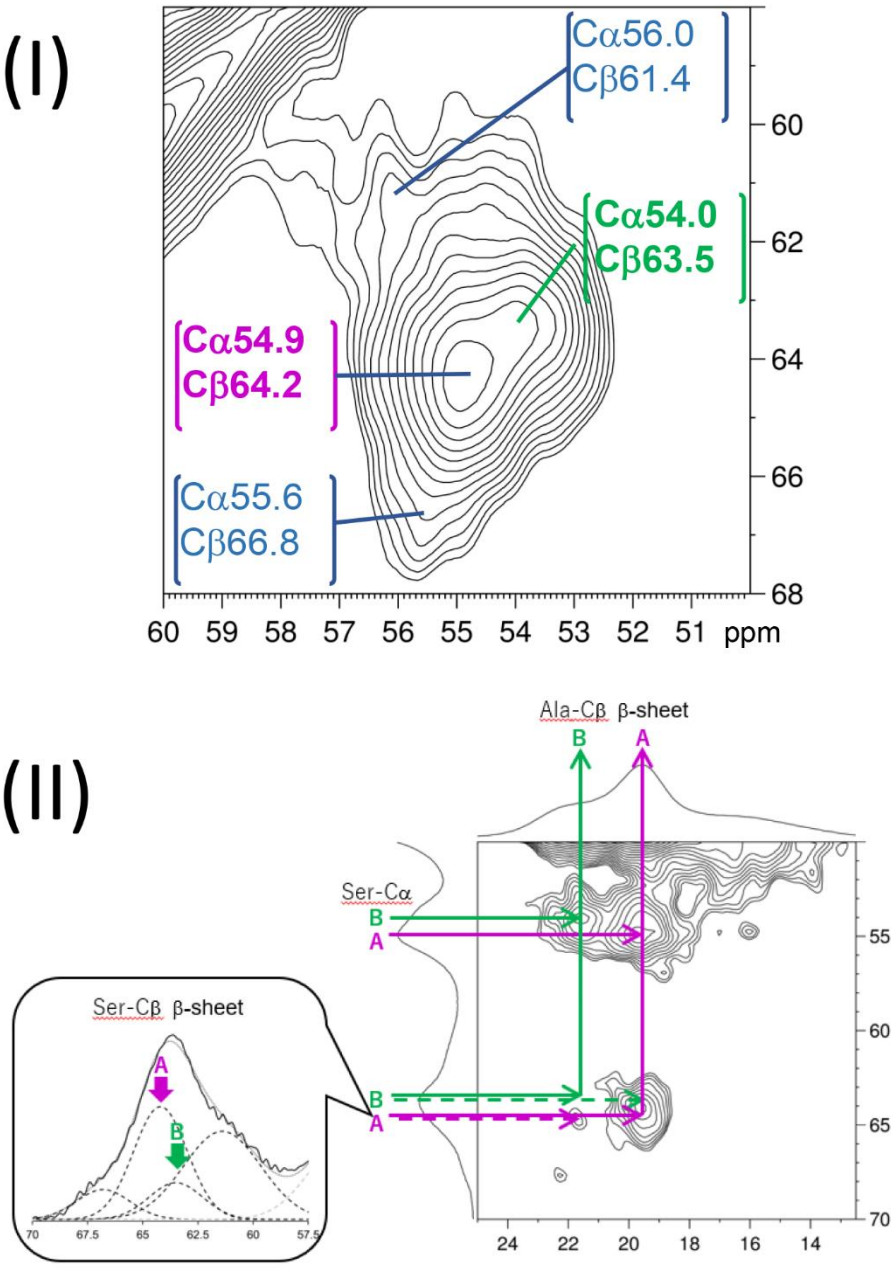

Figure 14. (I) Expanded Ser Cα-Cβ correlation from the 2D ^{13}C-^{13}C DARR spectrum of the [U-^{13}C] Cp fraction in the Silk II form observed with a mixing time of 10 ms. The peak assignment of four cross peaks is shown. (II) (Ala Cβ)-Ser Cα/Cβ) correlations in the 2D ^{13}C-^{13}C DARR spectrum of the [U-^{13}C] Cp fraction in the Silk II form observed with a mixing time of 400 ms. Solid lines show the correlations with the β-sheet carbons **A** and **B**. Adapted with permission from Okushita et al, Local Structure and Dynamics of Serine in the Heterogeneous Structure of the Crystalline Domain of Bombyx mori Silk Fibroin in Silk II Form Studied by 2D ^{13}C–^{13}C Homonuclear Correlation NMR and Relaxation Time Observation. Macromolecules 2014, 47, 4308−4316. Copyright 2014 American Chemical Society.

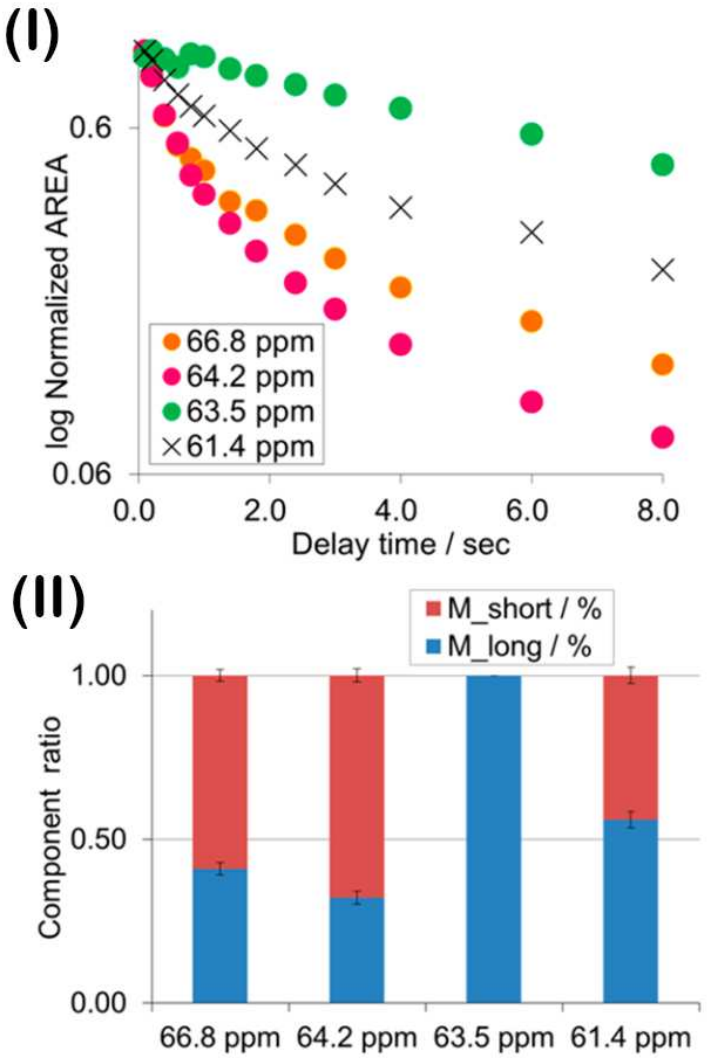

Figure 15. (I) Log plot of normalized area of each Ser Cβ peak observed in the T_1^c measurement of [3-^{13}C]Ser^{15}-(AGSGAG)$_5$ via Torchia's pulse sequence[106] versus delay time. (II) Stacked column chart of component ratios of shorter and longer T_1^c values for each Ser Cβ peak. Adapted with permission from Okushita et al, Local Structure and Dynamics of Serine in the Heterogeneous Structure of the Crystalline Domain of Bombyx mori Silk Fibroin in Silk II Form Studied by 2D ^{13}C–^{13}C Homonuclear Correlation NMR and Relaxation Time Observation. Macromolecules 2014, 47, 4308−4316. Copyright 2014 American Chemical Society.

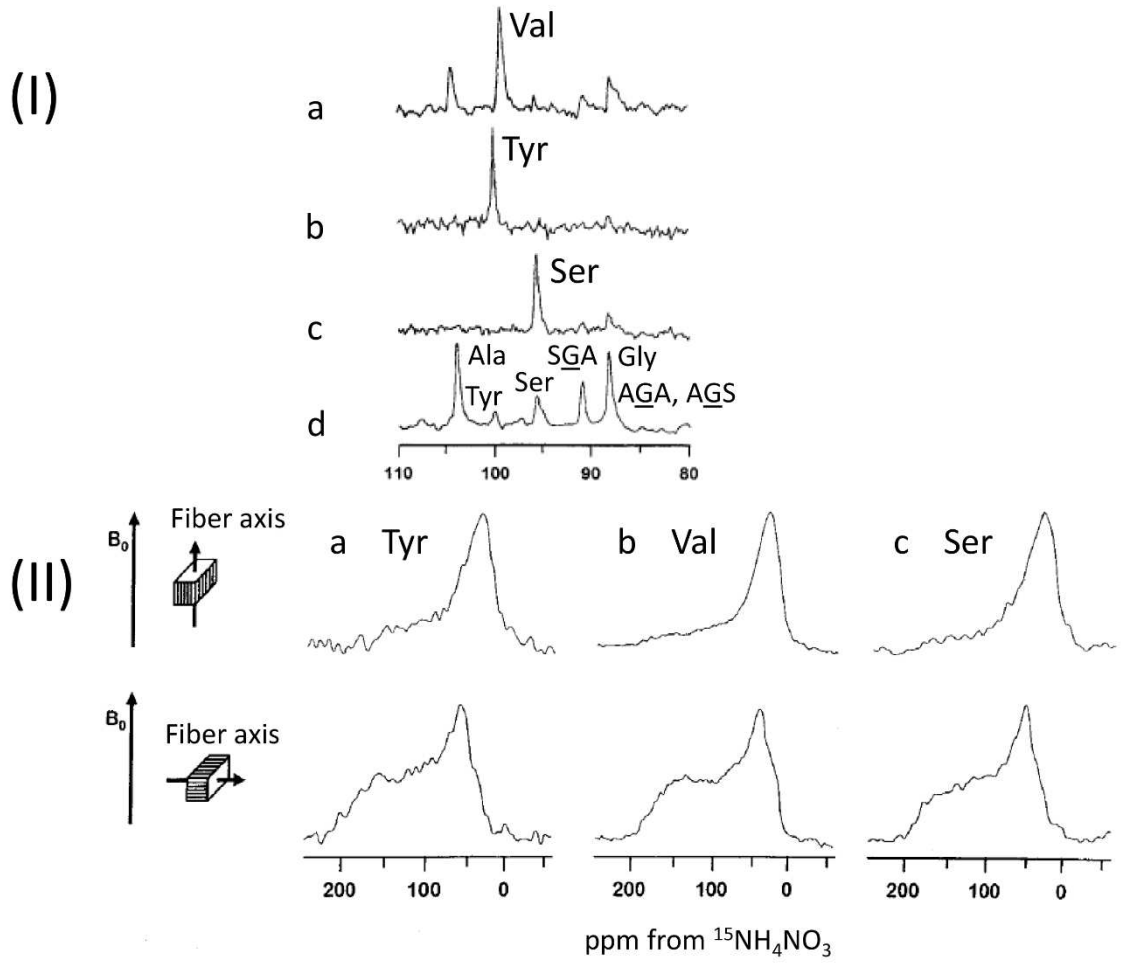

Figure 16. (I) ^{15}N solution NMR spectra (80-110 ppm) of selectively labeled SF fiber samples: (a) [^{15}N]Val-SF, (b)[^{15}N]Tyr-SF, and (c) [^{15}N]Ser-SF. For comparison, the ^{15}N NMR spectrum (d) of non-labeled (natural abundance) SF fiber is also shown. (II) ^{15}N solid state NMR spectra (0-200 ppm) of the labeled, uniaxially aligned SF fiber: (a) [^{15}N]Tyr-SF, (b)[^{15}N]Val-SF, and (c) [^{15}N]Ser-SF. The fiber axis was placed parallel (upper spectra) and perpendicular (lower spectra) to the static magnetic field direction B_0. Approximately 30% of the intensity arising from non-oriented powder patterns was subtracted from the experimental spectra. Adapted with permission from Asakura et al., Comparative Structure Analysis of Tyrosine and Valine Residues in Unprocessed Silk Fibroin (Silk I) and in the Processed Silk Fiber (Silk II) from *Bombyx Mori* Using Solid-State ^{13}C, ^{15}N, and ^{2}H NMR. Biochemistry 2002, 41, 4415–4424. Copyright 2002 American Chemical Society.

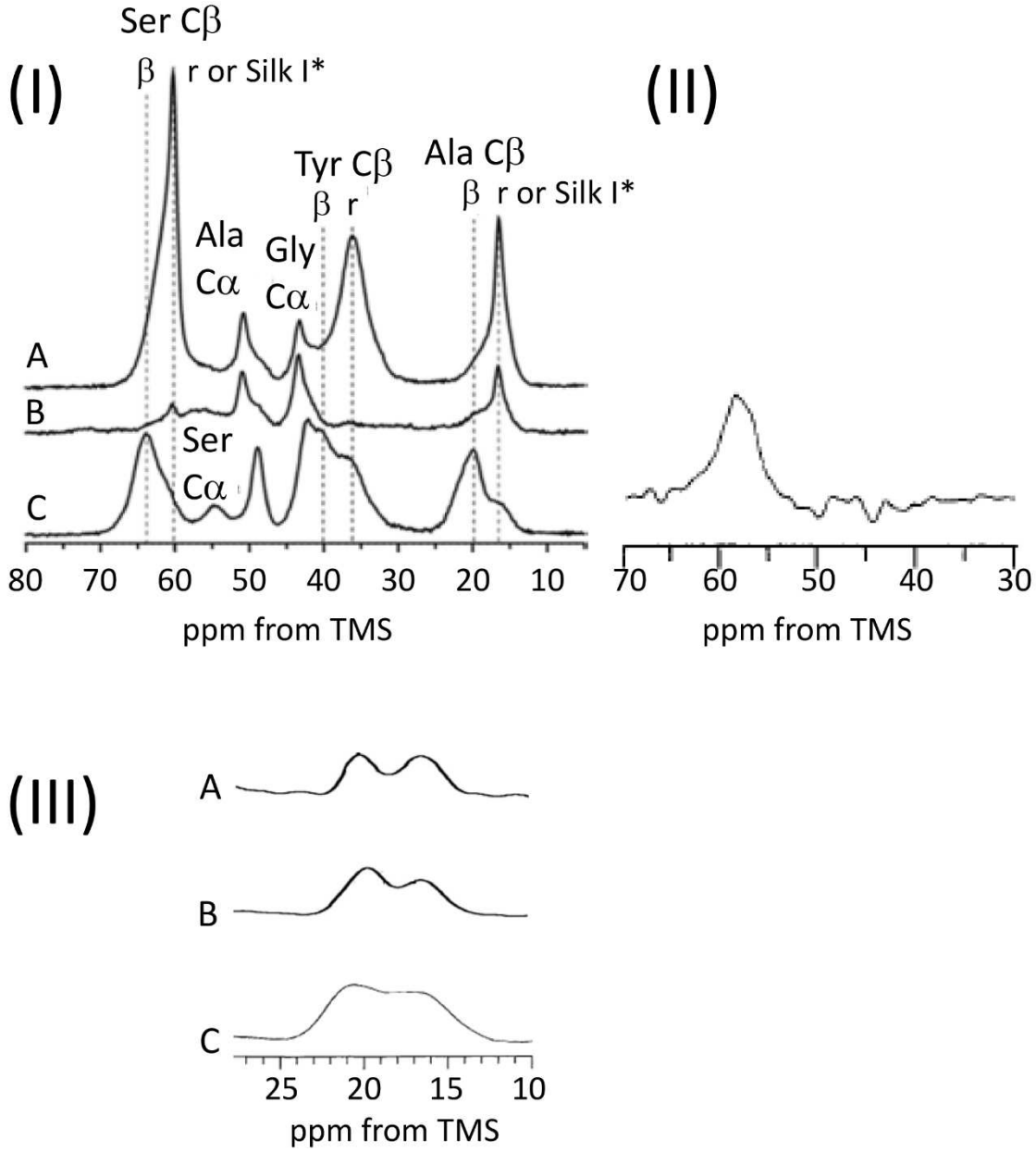

Figure 17. (I) Expansion of the 0−80 ppm region from the ^{13}C CP/MAS NMR spectra of SF. (A) ^{13}C-labeled Ser, Tyr, and Ala Cβ carbons of the SF before stretching. (B) Non-labeled carbons of the SF before stretching. (C) ^{13}C-labeled Ser, Tyr, and Ala Cβ carbons of the SF fiber in the Silk II form. Adapted with permission from Asakura et al., Stretching-Induced Conformational Transition of the Crystalline and Noncrystalline Domains of ^{13} C-Labeled *Bombyx Mori* Silk Fibroin Monitored by Solid State NMR. Macromolecules 2015, 48, 5761–5769. Copyright 2015 American Chemical Society. (II) Val ^{13}Cα peak in the ^{13}C CP/MAS NMR spectrum obtained by subtracting nonlabeled SF fiber from [2-^{13}C]Val-SF fiber. Adapted with permission from Asakura et al., Comparative Structure Analysis of Tyrosine and Valine Residues in Unprocessed Silk Fibroin (Silk I) and in the Processed Silk Fiber (Silk II) from *Bombyx Mori* Using Solid-State ^{13}C, ^{15}N, and ^{2}H NMR. Biochemistry 2002, 41, 4415–4424. Copyright 2002 American Chemical Society. (III) Expanded Ala Cβ peaks in the ^{13}C CP/MAS NMR spectra of (A) $(AGYGAG)_5$, (B) $(AGAGYGAGAG)_3$ and (C) $(AG)_3YG(AG)_2VGYG(AG)_3YG(AG)_3$ in the Silk II forms. Reprinted with permission from Asakura & Yao, ^{13}C CP/MAS NMR Study on Structural Heterogeneity in *Bombyx Mori* Silk Fiber and Their Generation by Stretching. Protein Sci. 2009, 11, 2706-2713 31,1529−1541. Copyright 2009 John Wiley and Sons.

Table 1. Atomic distances calculated from REDOR plots for five ^{13}C,^{15}N-labeled peptides: (D1) $(AG)_7[^{15}N]A^{15}[2\text{-}^{13}C]G^{16}(AG)_7$; (D2) $(AG)_7A[^{15}N]Gly^{16}[2\text{-}^{13}C]Ala^{17}G\text{-}(AG)_6$; (D3) $(AG)_6A[1\text{-}^{13}C]Gly^{14}A[^{15}N]Gly^{16}(AG)_7$; (D4) $(AG)^7[1\text{-}^{13}C]Ala^{15}G[^{15}N]\text{-}Ala^{17}G(AG)_6$; (D5) $(AG)_7[^{15}N]Ala^{15}[1\text{-}^{13}C]Gly^{16}(AG)_7$. Adapted with permission from Asakura et al., Lamellar Structure in Poly(Ala-Gly) Determined by Solid-State NMR and Statistical Mechanical Calculations. J. Am. Chem. Soc. 2007, 129, 5703-5709. Copyright 2007 American Chemical Society.

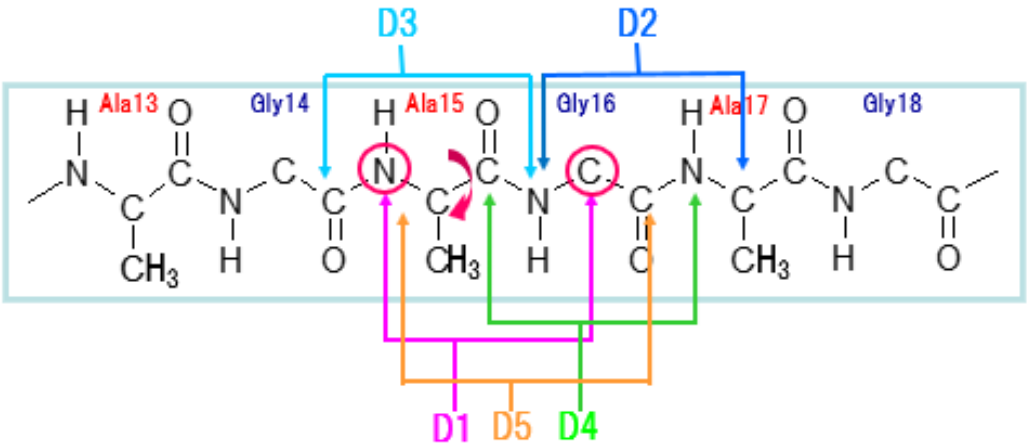

	labeled site	observed distances (Å)	β-sheet (Å)	β-turn (Å)	simulated distances (Å)
D1	$[^{15}N]Ala^{15}\cdots[2\text{-}^{13}C]Gly^{16}$	4.6 ± 0.1	4.82	4.74	4.8
D2	$[^{15}N]Gly^{16}\cdots[2\text{-}^{13}C]Ala^{17}$	4.7 ± 0.1	4.96	4.17	4.8
D3	$[1\text{-}^{13}C]Gly^{14}\cdots[^{15}N]Gly^{16}$	4.5 ± 0.1	4.77	3.85	4.6
D4	$[1\text{-}^{13}C]Ala^{15}\cdots[^{15}N]Ala^{17}$	4.5 ± 0.1	4.76	2.94	4.4
D5	$[^{15}N]Ala^{15}\cdots[1\text{-}^{13}C]Gly^{16}$	5.2 ± 0.3	6.02	5.05	5.8

Table 2. T_1^C Relaxation Times (T_1^C(short/s) and T_1^C(long/s) of [3-^{13}C]Ser^{15}-(AGSGAG)$_5$ and their fractions (I (short) and I (long)), respectively for four peaks of Ser Cβ carbon. Adapted with permission from Okushita et al, Local Structure and Dynamics of Serine in the Heterogeneous Structure of the Crystalline Domain of Bombyx mori Silk Fibroin in Silk II Form Studied by 2D ^{13}C–^{13}C Homonuclear Correlation NMR and Relaxation Time Observation. Macromolecules 2014, 47, 4308−4316. Copyright 2014 American Chemical Society.

	66.8 ppm	64.2 ppm	63.5 ppm	61.4 ppm
I (short)	0.59	0.68		0.44
I (long)	0.41	0.32	1.00	0.56
T_1^C (short/s)	0.32	0.45		0.73
T_1^C (long/s)	4.92	4.43	10.75	8.43